IEEE Access
Multidisciplinary | Rapid Review | Open Access Journal

Received 12 December 2022, accepted 30 December 2022, date of publication 4 January 2023, date of current version 11 January 2023.

Digital Object Identifier 10.1109/ACCESS.2023.3234043

RESEARCH ARTICLE

Enhancing the Conventional Controllers for Load Frequency Control of Isolated Microgrids Using Proposed Multi-Objective Formulation via Artificial Rabbits Optimization Algorithm

A. ELSAWY KHALIL, TAREK A. BOGHDADY, M. H. ALHAM, AND DOAA KHALIL IBRAHIM, (Senior Member, IEEE)
Electrical Power Engineering Department, Faculty of Engineering, Cairo University, Giza, Cairo 12613, Egypt
Corresponding author: M. H. Alham (moh.alham@eng.cu.edu.eg)

ABSTRACT Isolated microgrids (IMGs) power remote areas. However, IMG may lower the frequency stability and increase frequency excursions with low system inertia. Load frequency management ensures system stability. Thus, the paper proposes a novel multi-objective tuning strategy to improve IMG's load frequency control (LFC) and take the microgrid controller's control signals into account. Diesel engine generator, fuel cell, battery energy storage system, and renewable energy sources (RESs) like photovoltaic and wind systems make up the IMG. Conventional controllers such as proportional-integral (PI) and proportional integral derivative (PID) are classically tuned based on the standard error criteria as a traditional single-objective tuning approach. Due to the low inertia of the system and the stochastic nature of RES, they cannot act as required under different operating scenarios. Therefore, the PI and PID controllers are tuned using the proposed multi-objective-based tuning approach to reduce the frequency deviations. In addition, anti-windup is applied to the enhanced classic controllers to keep them distant from the nonlinear zone and beyond the source's physical constraints. The proposed tuning process also considers the maximum practical generation rates for different sources. The recent Artificial Rabbits Optimization (ARO) algorithm is applied to simultaneously adjust the controller parameters for several controlled sources in IMG. Extensive simulations in MATLAB and Simulink confirm the effectiveness of the proposed approach to keep the system stable even when facing high levels of disturbances. In addition, accomplishing sensitivity analysis, severe $\pm 25\%$ changes to the system's parameters guarantee that the proposed tuning strategy keeps the system stable.

INDEX TERMS Artificial rabbits optimization (ARO) algorithm, isolated microgrid (IMG), load frequency control (LFC), multi-objective tuning approach, renewable energy resources (RES).

LIST OF ABBREVIATIONS

ARO	Artificial Rabbits Optimization.
BESS	Battery Energy Storage System.
DEGs	Diesel Engine Generators.
DGUs	Distributed Generating Units.
DR	Decay Ratio.
ESSs	Energy storage systems.
FCs	Fuel Cells.
FO	Fractional Order.
GA	Genetic Algorithm.
GRC	Generation Rate Constraint.
GWO	Grey Wolf Optimization.
IAE	Integral Absolute Error.
IMG	Isolated Microgrid.
ISE	Integral Square Error.
ITAE	Integral Time Absolute Error
ITSE	Integral Time Square Error.

The associate editor coordinating the review of this manuscript and approving it for publication was Md. Abdur Razzaque.

LFC	Load Frequency Control.
MBA	Mine Blast Algorithm.
MFO	Moth Flame Optimizer.
MGs	Microgrids.
OSH	Overshoot.
PI	Proportional-Integral.
PID	Proportional-Integral-Derivative.
PSO	Particle Swarm Optimization.
PV	Photovoltaic.
RESs	Renewable Energy Sources.
SMA	Slime Mould Optimization Algorithm.
SMES	Super Magnetic Energy Storage.
Ts	Settling Time.
USH	Undershoot.
WOA	Whale Optimization Algorithm.
WT	Wind Turbine.

I. INTRODUCTION

Microgrids (MGs) have two operating modes; isolated mode and grid-tied mode. The grid-tied operation promises the balance between generation and load and has a supportive role in mitigating load disruption. Isolated microgrids (IMGs) require inventive structures and adaptable control mechanisms for performance and stability [1]. Two types of IMGs are often in low and medium-voltage networks. The first type is the single-area [2], whereas the second is the multi-area [3]. IMG is extended by adding energy storage systems (ESSs), like fuel cells (FCs) and battery energy storage systems (BESSs) [4], [5], to ensure the robustness and reliability of IMG against load disturbance with the shortage in conventional distributed generating units (DGUs). Recently, renewable energy sources (RES), such as photovoltaic (PV) modules and wind turbines (WTs) [6], controlled loads, and ESSs are combined with conventional diesel engine generators (DEGs) [7] to create the current IMG structure [2], [3], [8], [9]. In addition to IMG's inertia restrictions, inverter-based devices with modern IMG structures reduce the overall system inertia [10]. RES uncertainty also jeopardizes frequency stability, especially in single-area IMG [11]. As a vital supplemental service in IMGs, the load frequency control (LFC) scheme improves frequency stability [12], [13].

Numerous traditional and new controllers, adjusted using different tuning methodologies, have been employed to explore the LFC schemes of the single and multi-area IMGs. As reported in the literature, still the LFC can be achieved by using conventional controllers with straightforward designs and high robustness, like proportional-integral (PI) and proportional-integral-derivative (PID). However, improper PI/PID controller tuning may cause poor dynamic behavior and instability throughout the system [14]. As a result, the tuning and design approaches are significant factors in providing reliable controllers and guaranteeing overall system stability [15], [16].

Generation units have physical limitations that result in intrinsic generation rate constraints (GRC), such as ramp rate constraints and upper-lower bound constraints. Lack of effective GRC in LFC design can lead to poor controller performance and limited closed-loop system stability in the presence of disturbances [17], [18], [19]. Moreover, the anti-windup property keeps traditional controllers out of the nonlinear zone [20] and away from the source's physical restrictions, especially in the LFC scheme for nonlinear systems [21].

There have been significant efforts in the last decade to tune classical controllers properly in a variety of engineering problems, including those corresponding to the automatic generation control of IMGs, whether in the field of automatic voltage regulation [22], [23] or LFC schemes [24], [25], [26], [27], [28], [29], [30], [31], [32], [33]. The slime mould optimization (SMA) algorithm is proposed in [24] to improve the frequency stability of a two-area IMG with thermal and photovoltaic units using a single objective formulation to determine the PI controller's optimal parameters. The LFC problem and tuning procedure were made by the thermal unit's high inertia and the preset PV system profile, which made the IMG less uncertain, and the GRC of thermal unit is not considered. The LFC of two-area IMG is also investigated in [25], whereas PI controller parameters are tuned using a single objective approach based on the artificial sheep algorithm. Such IMG has reheated thermal units with a PV unit besides hydro-pumped storage. Reheated thermal units' GRC is considered, but the controller's effectiveness is tested in a high-inertia IMG with a high-power density supply, like pumped storage, to minimize traditional controllers' uncertainty constraints. In [26], the firefly and particle swarm optimization, as a hybrid optimization technique, is presented to tune the parameters of a standard PID controller of a single-area IMG that contains a flywheel. For such low inertia IMG, the authors overcome ignoring the GRC of DEG by employing the flywheel to mitigate the uncertainty due to the WT used. The mine blast algorithm (MBA) is described in [27] and [28] for tuning PID controllers and enhancing LFC of low inertia single-area IMG that includes super magnetic energy storage (SMES) and also a multi-area IMG has ultra-capacitor, respectively. Single objective tuning is applied without considering GRC to adjust the controllers' optimal gains where ultra-capacitors and SMES provide a durable network and make it easier to tune multiple controllers in the LFC manner. Without sources of a high-power density and considering sources' GRC, these MGs cannot assess controller effectiveness. Thus, the authors suggested a multi-objective-based tuning strategy to maximize controllers' significance with no high-power density sources. In [29], [30], and [31], a method for LFC for both single and multi-area IMGs is proposed using conventional PI, PID, and fuzzy-based PID controllers. The optimum traditional controller tuning for the LFC is presented based on numerous single objective error criteria that various optimization techniques have optimized. In [29], the moth flame optimizer (MFO) tunes controller parameters without considering sources' GRC of reheat-thermal units of two-area IMG. In [30] and [31], the grey wolf optimization algorithm (GWO)

and whale optimization algorithm (WOA) took the sources' GRC into account. Despite the authors' consideration of GRC during tuning in [30] and [31], the simple single objective tuning is utilized with high inertia sources, and the efficiency of proposed LFC techniques is not verified for low inertia IMG.

On the other hand, simplifying tuning methods and addressing the nonlinear system limits of conventional controllers can be achieved with some advanced controllers, such as fuzzy-based PID and fractional order (FO) controllers, which may replace traditional ones. For example, the type-II fuzzy PID controller was provided by [32] to give LFC of two-area IMGs comprising microturbine and flywheels. That work uses the improved-slap swarm optimization to find the optimal gains for the PID controller using a single-objective tuning without considering the DEGs unit's GRC. In low inertia MGs with the absence of high-power density sources, many sophisticated controllers based on single-objective tuning processes may fail if the sources' GRC is ignored.

Some research studies did not address GRC during controller tuning [24], [26], [27], [28], [29]. Thus, these approaches have no theoretical basis for efficacy. On the other hand, [25], [30], [31] have addressed GRC in LFC. Unfortunately, neither of these studies has overcome MG's lack of inertia. These LFC schemes work best with structures that use high-power density or high-inertia sources, while they are not successful in demonstrating their efficacy when used with weak structures such as the low inertia single-area IMG.

The authors believe there is room to create viable strategies for adapting traditional controllers for low-inertia IMGs. A multi-objective tuning method based on the Artificial Rabbits Optimization (ARO) algorithm is proposed for PI and PID controllers. The research's main findings are:

1. Offering a novel multi-objective-based tuning technique that incorporates the integral square error (ISE) as one of the most often used error criteria, the control signals from several sources, and finally, the settling time as a vital issue in the LFC scheme of IMGs.
2. Using the ARO algorithm, a recent optimization algorithm introduced in 2022, to simultaneously tune the controller settings for a range of controlled sources to enhance IMG frequency stability.
3. Compared to the structures in the literature that use either high power density or high inertia sources, using the proposed formulation for low-inertia IMG can be seen as a real challenge.
4. Discussing the role of GRC as a significant system issue encompasses physical factors from multiple sources, which are not addressed sufficiently in the literature. When employed to control nonlinear systems, linear controllers' anti-windup property also helps improve their stability.

The paper will be structured as follows: Section II introduces the planned IMG's architecture with several sources and the controllers' structures. Section III presents the proposed problem formulation. In Section IV, the optimization algorithm is explained. Section V compares the outcomes of employing the suggested multi-objective formulation to some reported criteria, and Section VI introduces the sensitivity analysis. Section VII highlights the conclusions and future work.

II. MODELING OF THE TESTED ISOLATED MICROGRID

Numerous MG models are investigated in [1], where the first-order dynamic models are adequate and simple for LFC representations over higher-order dynamic models. The first-order dynamic models for DGUs are straightforward to avoid the aggregate complication of MGs and are also suitable for the LFC scheme [34], [35], [36], [37]. Consistent with recent research, the authors have applied uncomplicated first-order transfer functions to represent DGUs in the considered IMG.

The studied IMG is depicted in Fig. 1 with the contributing elements. Storage elements are modeled using the fuel cell (FC) and the battery energy storage system (BESS) models to provide enough energy to support load frequency stability. Wind and PV systems present renewable energy sources (RES) in this IMG, which are uncontrolled sources to facilitate other sources in different load disturbances. Three different conventional controllers are used for the LFC scheme by the reminder sources of the IMG, which are the controlled sources of diesel engine generator (DEG), FC, and BESS.

The following subsections present the model of DEG as a fast-active power supply for the IMG. Dynamic models of BESS and FC are also demonstrated. Due to the widespread collaboration of wind turbines and PV systems in the LFC scheme, a dynamic model is presented for each RES. Then, the overall MG dynamic model is discussed. Lastly, the structure of the studied controllers is briefly described.

A. DIESEL ENGINE GENERATOR MODEL

DEG is a reliable and quick source of durable electric power generation through load perturbation [35]. The assigned transfer function used for the DEG model via frequency control scheme is presented in Fig.1. A governor and a generator specified by the first-order plant model often make up this model. The system also includes a turbine to represent the inertia delay. The DEG output power variation can be represented as follows:

$$\Delta P_{DEG} = \left(\frac{1}{sT1+1} \times \frac{1}{sT2+1} \times \frac{1}{sT3+1}\right) \times \left(\frac{-1}{R}\Delta F - \Delta U_{DEG}\right) \quad (1)$$

In equation (1), the terms $T1$, $T2$, and $T3$ stand for the Inertia delay time constant, governor time constant, and generator time constant, respectively. The symbol ΔF refers to frequency fluctuation. The DEG speed regulation coefficient is displayed by R, while ΔP_{DEG} denotes the amount of DEG power variation during disturbances and ΔU_{DEG} is the control signal of DEG. The secondary loop adopts the DEG

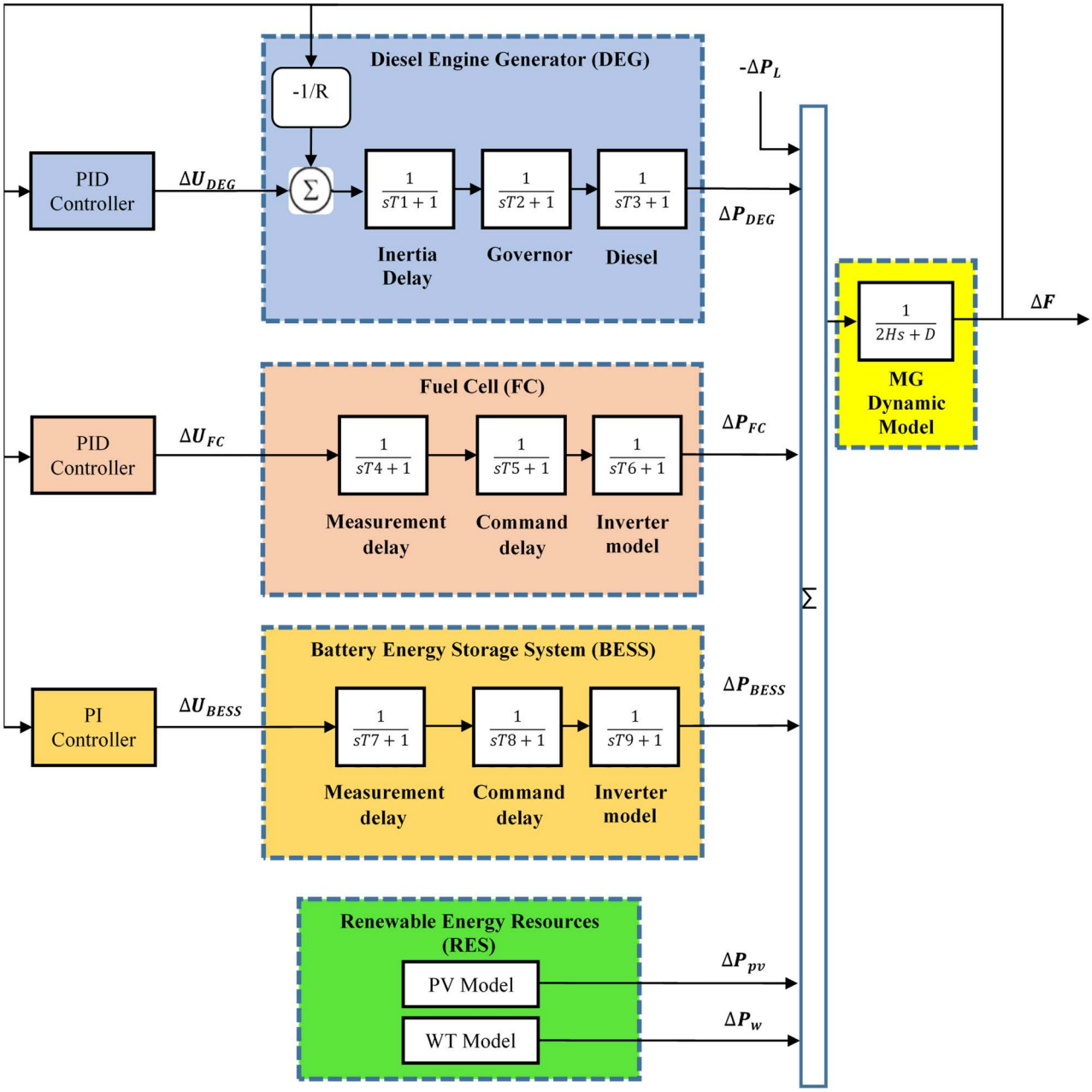

FIGURE 1. The tested IMG.

power mismatches with the addition of a conventional PID controller.

B. FUEL CELL MODEL

As discussed in [38], the FC model can be established with three first-order transfer functions. This model provides sufficient small signal stability for the LFC analysis. It consists of three basic blocks: an inverter block that converts DC voltage to AC voltage; an interconnection device with two primary blocks, one for modeling the measurement delay and the other for command delay as revealed in Fig. 1. The output power of FC employed in the LFC scheme can be modeled as follows:

$$\Delta P_{FC} = \left(\frac{1}{sT4+1} \times \frac{1}{sT5+1} \times \frac{1}{sT6+1}\right) \times (-\Delta U_{FC}) \tag{2}$$

where ΔP_{FC} stands for FC active power variation during system disturbances, ΔU_{FC} for the FC control signal, $T4$ for the measurement time delay, $T5$ for the command device delay, and $T6$ for the inverter model time constant. In the current frequency control scheme, FC is controlled by a conventional PID controller.

C. BATTERY ENERGY STORAGE MODEL

For the proposed LFC, BESS performs as an ancillary source that contributes to power generation during disturbance and steady-state operations. According to [39], BESS is used in conjunction with a battery energy management system. The authors assume that the battery is functioning within a normal range. The load, which consumes a range of permissible currents at a fixed rated output voltage, is the main characteristic of the normal zone.

As depicted in Fig. 1, it is critical to consider all time delays; measurement delay, command delay, and converter delay.

For the current LFC model, BESS output power can be modeled as follows:

$$\Delta P_{BESS} = \left(\frac{1}{sT7+1} \times \frac{1}{sT8+1} \times \frac{1}{sT9+1}\right) \times (-\Delta U_{BESS}) \quad (3)$$

In equation (3), $T7$ is the measurement time constant, $T8$ is the command device delay, $T9$ is the DC to AC converter model time constant, ΔU_{BESS} is the control signal of BESS and ΔP_{BESS} characterizes the change in BESS shared active power during system variations. It is worth mentioning that in the present LFC scheme, BESS is controlled by a conventional PI controller.

D. MODELS OF RENEWABLE ENERGY SOURCES

In the following subsections, the models presenting PV and WT will be briefly discussed.

1) PV MODEL

Basically, the output power of a PV system depends on solar radiation, PV panel efficiency, panel size, and ambient temperature. The extracted output power of the PV system can be presented as follows [39]:

$$pv\,(s) = \eta_{pv} \times A_{pv} \times S \times [1 - 0.0005 \times (T_0 - 25)] \quad (4)$$

where η_{pv} defines the efficiency of the PV system, S is the solar radiation, A_{pv} is the area of the PV system, and T_0 is the cell temperature.

The white noise block in Fig. 2 represents the stochastic character of PV generation, whereas $T10$ is the delay time constant and ΔP_{PV} is the amount of PV power variation throughout the simulation.

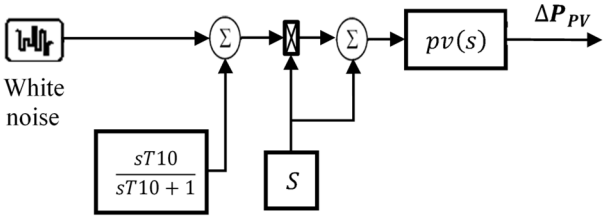

FIGURE 2. PV model.

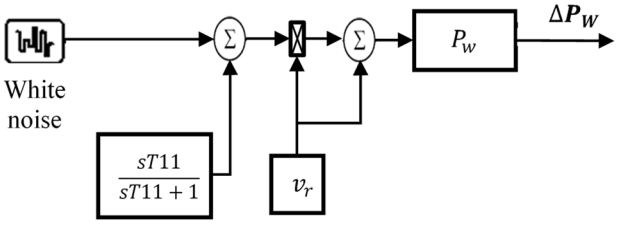

FIGURE 3. Wind turbine model.

2) WIND MODEL

The following equation defines how the wind turbine generates power by harnessing the kinetic energy of the air [40]:

$$P_w = 0.5 v_r^3 A_w \rho_{air} C_p\,(\gamma.\beta) \quad (5)$$

where P_w describes the wind turbine output power, v_r is the rated speed of the wind, A_w is the rotor swept, and C_p denotes the performance coefficient of rotor blades. The approximate equation of the performance coefficient can be in terms of turbine coefficients C_1– C_7 as follows [40]:

$$C_p\,(\gamma.\beta) = C_1 \times \left(\frac{C_2}{\gamma_i} - C_3\beta - C_4\beta^2 - C_5\right) \times e^{-\frac{C_6}{\gamma_i}} + C_7\gamma_t$$
$$and\ \gamma_t = (w \times r)/v_r \quad (6)$$

Referring to equation (6), β designates the pitch angle, γ_i is the intermittent tip speed ratio, and γ_t is the optimum tip speed. The rotor blade radius is described by r, and w is the rotational speed of the blades.

The equation that describes the intermittent tip speed ratio is expressed as shown:

$$\gamma_i = \frac{(\beta^3 + 1) \times (\gamma_t + 0.08\beta)}{(\beta^3 + 1) - 0.035 \times (\gamma_t + 0.08\beta)} \quad (7)$$

Figure 3 illustrates the details of the simple block shown in Fig.1 for wind turbine power generation in the LFC scheme. The stochastic behavior of wind energy generation is offered by a white noise block while $T11$ describes the delay time constant, and ΔP_W defines the amount of wind turbine power variation along simulation time.

E. MICROGRID DYNAMIC MODEL

The DEG, FC, BESS, RES, and MG load are the five subsystems that make up the IMG described in Fig. 1. The following formula can be used to determine the frequency variation of that IMG:

$$\Delta F = \frac{1}{2Hs + D}\,(\Delta P_{DEG} \pm \Delta P_{FC} \pm \Delta P_{BESS} + \Delta P_{RES} - \Delta P_L) \quad (8)$$

Referring to equation (8), ΔF defines the MG frequency variation, H is the overall inertia constant of the system, D is the load damping coefficient, ΔP_L is the variation in load, ΔP_{DEG} is the variation in DEG power generation, ΔP_{FC} is the variation in output power of FC, ΔP_{BESS} is the variation in output power of BESS, and ΔP_{RES} is the variation in RES

output power. The variation in RES output power is the sum of the variation of PV and WT output power i.e. $\Delta P_{RES} = \Delta P_{PV} + \Delta P_W$.

F. APPLIED CONTROLLERS

1) PI-CONTROLLER

PI controllers are still frequently used in industry due to their straightforward design and adequate performance for most industrial applications. The proportional and integral gains are the two primary tuning parameters for this controller. Equation (9) shows the Laplace transform to express the transfer function (TF) of the PI-controller:

$$TF(s)_{PI} = K_p + K_i \frac{1}{s} \tag{9}$$

where K_p and K_i are the proportional and integral gains, respectively, which can be optimally tuned using numerous optimization algorithms to enhance the LFC problem.

2) PID-CONTROLLER

PID controllers are PI controllers modified to incorporate a derivative term to improve the dynamic response of the controlled systems. PID has excellent dynamics and robust properties, which is regarded as one of the most flexible feedback controllers [41].

PID controllers rely on proportional, integral, and derivative gains (K_p, K_i, and K_d). So, to keep the stability of system frequency in MG, these gains should be optimally tuned using an efficient computing technique. In the Laplace transform, the TF of a PID controller is introduced as follows:

$$TF\ (s)_{PId} = K_p + K_i \frac{1}{s} + K_d s \tag{10}$$

III. PROPOSED MULTI-OBJECTIVE TUNING APPROACH

A. FORMULATION

The appropriate choice of the employed objective function in the LFC scheme has a crucial impact on the controller's performance [8], [41]. Numerous objective functions, either single objective [25], [42], [43], or multi-objective [44], [45], [46] have been developed in earlier studies to reduce the frequency deviation of an IMG. Most of these studies use one of the widely accepted error criteria to enhance frequency stability. Such as the integral absolute error (IAE), the integral time absolute error (ITAE), the integral square error (ISE), or the integral time square error (ITSE).

Although these criteria produced good performance indices, they do not always ensure that all performance indices will be improved, e.g., the ITAE criterion provides better settling time more sensitive than other criteria such as ISE. However, the optimal tuning-based ITAE can result in a large control signal that may be hazardous in the sudden imbalance [47]. On the contrary, the ISE criterion punishes errors with large values against lesser errors [48]. The control error's large values usually occur instantly after a step disturbance and may be represented as the system overshoot [48]. Due to the benefits of aggressive control mitigation via weak IMG, the ISE criterion is still often utilized in LFC difficulties even though it has long settling periods and is typically used to measure direct overshoot and violent control.

Researchers have also used the common error criteria to optimize several controller types for isolated networks and concluded that ISE has the potential to offer overall superior performance to other controller types, especially for low inertia IMG [33], [49], [50]. As a result, the ISE error criterion will be selected in this research to tune the various controllers of the studied IMG's LFC scheme. Additionally, in this research, the tuning procedure is carried out by utilizing a multi-objective function that aggregates many objectives to provide an effective LFC scheme.

The first objective function J_1 is ISE, it might be easier to be traced mathematically as follows:

$$J_1 = ISE = \int_0^{t_{sim}} (\Delta F)^2 dt \tag{11}$$

where ΔF is the frequency deviation to be minimized and t_{sim} is the simulation time.

More improvement in ISE necessitates high control signals from different controllers for the LFC scheme to moderate various system disturbances effectively. However, this raises the settling time, which is considered a significant performance metric. Directly including settling time as a term in a multi-objective function has a large positive impact on the settling time but a negative impact on other performance indicators [38], [51]. Thus, this research will also use an indirect novel technique by reducing the square of the control signal based on the system's output feedback, or ΔF, besides the addition of the settling time and ISE in the overall multi-objective function.

Reduction control signals will direct the various sources' outputs when there are large disturbances, preventing different controllers from reacting aggressively to disturbances, which indirectly helps to improve the settling time. So, the second objective in the suggested multi-objective function will be expressed as follows, which is the integral square of control signals from various controlled sources.

$$J_2 = \int_0^{t_{sim}} (\Delta U_{DEG}^2 + \Delta U_{BESS}^2 + \Delta U_{FC}^2) dt \tag{12}$$

In equation (12), ΔU_{DEG}, ΔU_{BESS}, and ΔU_{FC} describe the control signals of DEG, BESS, and FC, respectively.

Finally, since the settling time is a key index in the IMG LFC scheme, it is directly used as the third objective in the proposed multi-objective function as follows, where Ts is the time taken by the system to settle at $\Delta F = 0$:

$$J_3 = Ts \tag{13}$$

The combined multi-objective function J in equation (14) consists of three individual functions; J_1, J_2, and J_3 which can be formulated as follows:

$$J = w_1 \cdot J_1 + w_2 \cdot J_2 + w_3 \cdot J_3 \tag{14}$$

The weighting factors representing each function's effectiveness and contribution in the proposed multi-objective function J are described by w_1, w_2, and w_3 for ISE, the control signals, and settling time, respectively. Based on the weighted sum multi-objective approach [52], the sum of all weighting factors can be signified as follows:

$$\sum_{i=1}^{3} w_i = 1 \tag{15}$$

The optimal weighting values vary depending on system dynamics, and accordingly, the network operators select the best method to adjust each controller in the LFC scheme. Equal weighting is the simplest method for determining the weighting factors. So, in this study, it is assumed that all weighting factors are the same, i.e., $w_1 = w_2 = w_3 = 1/3$.

The inequality constraints of the proposed multi-objective function are represented by:

$$\begin{aligned} K_p^{min} &\le K_p \le K_p^{max} \\ K_i^{min} &\le K_i \le K_i^{max} \\ K_d^{min} &\le K_d \le K_d^{max} \end{aligned} \tag{16}$$

Regarding equation (16), K_p^{min}, K_i^{min}, K_d^{min} and K_p^{max}, K_i^{max}, K_d^{max} symbolize the minimum and maximum gains limits for the proportional, integral, and derivative parameters of various source controllers, respectively.

Zeigler-Nicholas's ultimate tuning approach [41] is used for setting the minimum and maximum limits of the PI and PID parameters in this study.

B. NORMALIZING AND SCALING

It is essential to normalize and scale different objectives since the range of each target should be changed in the same order to apply the optimization issue correctly.

1) NORMALIZING

Comparing several cost functions is one of many multi-objective optimization strategies. Comparing values from various objectives can be challenging since they may have different units and magnitudes. As a result, it is usually crucial to transform the objective functions into similar orders of magnitude. Although there are many normalization methods, the min-max strategy is the most dependable [53], allowing all normalized targets to fall between 0 and 1. The formula is outlined as follows:

$$F_{in} = \frac{F_i - F_{i_{min}}}{F_{i_{max}} - F_{i_{min}}} \tag{17}$$

where F_{in} is the normalized value of i^{th} objective function, $F_{i_{min}}$ and $F_{i_{max}}$ are the minima and maximum values of i^{th} objective.

Using equation (17), the proposed multi-objective function in equation (14) is reformulated to be:

$$J = w_1 \cdot J_{1n} + w_2 \cdot J_{2n} + w_3 \cdot J_{3n} \tag{18}$$

where J_{1n}, J_{2n}, and J_{3n} are the normalized values of J_1, J_2, and J_3, respectively. These normalized values can be estimated by the following formulas to become in the range of (0, 1):

$$J_{1n} = \frac{J_1 - J_{1min}}{J_{1max} - J_{1min}} \tag{19}$$

$$J_{2n} = \frac{J_2 - J_{2min}}{J_{2max} - J_{2min}} \tag{20}$$

$$J_{3n} = \frac{J_3 - J_{3min}}{J_{3max} - J_{3min}} \tag{21}$$

where $J_{1min}, J_{2min}, J_{3min}$ and $J_{1max}, J_{2max}, J_{3max}$ are the minimum and maximum values of J_1, J_2, and J_3, respectively.

Through three runs, each with 50 search agents and a total of 500 iterations, the authors have determined the minimum values of J_1, J_2, and J_3. The maximum value of J_1 is determined by the open loop response, the maximum value of J_2 is determined at the maximum spinning reserve by equation (12), and finally, the maximum stable value of J_3 is taken by the simulation time.

2) SCALING

Although the normalizing method guarantees that all objective values will fall within the range (0,1), it cannot ensure that all objectives will change in the same order while still falling within this range.

For example, when $J_{1n} = 1.5 \times 10^{-5}$, $J_{2n} = 2.2 \times 10^{-2}$, and $J_{3n} = 3.5 \times 10^{-2}$ and by normalizing them, all values are less than 1, but J_{1n} changes in the order of 10^{-5} while J_{2n} and J_{3n} change in order 10^{-2}, so J_{1n} must be scaled by multiplying 10^3 or dividing by 10^3 for J_{2n} and J_{3n} to be scaled. Right scaling makes it possible for optimization processes to fairly compare several objective functions, as in the previous example, when the optimization process does not disregard J_{1n} relative to others.

Consequently, the final formulation of the suggested objective function, derived from equation (18), will be as follows:

$$J = w_1 \cdot \alpha \cdot J_{1n} + w_2 \cdot \beta \cdot J_{2n} + w_3 \cdot \gamma \cdot J_{3n} \tag{22}$$

where α, β, and γ designate the scaling factors for J_{1n}, J_{2n}, and J_{3n} respectively. In our study we make 10 different runs, each one with 200 iterations to trace the average change order of all objective functions, then the scaling factors are decided to be as follows $\alpha = \gamma = 1000$, and $\beta = 1$.

IV. ARTIFICIAL RABBITS OPTIMIZATION (ARO)

A. SELECTION ARO AS THE OPTIMIZATION TECHNIQUE

Traditional optimization algorithms only solve convex problems. It can transform non-convex problems into convex ones within certain approximations [54]. Metaheuristic techniques are better than approximations to convert the existing non-linear and non-convex problem to a convex one before optimizing it using conventional methods. Numerous metaheuristic methods are utilized in literature to evaluate the LFC problem in recent studies [24], [25], [26], [27], [28], [29], [30], [31], [55], [56]. Artificial rabbits optimization (ARO)

is one of the most recent metaheuristic methods in 2022. According to [57], the ARO approach demonstrates the superiority of optimization over a variety of well-known metaheuristic techniques, including particle swarm optimization, differential evolution, gravitational search algorithm, cuckoo search, teaching–learning-based optimization, artificial bee colony, and atom search optimization. ARO meets the Global Search Convergence theorem. The theorem declares ARO cannot miss the global optimum. As a result, the optimization problem in this study is solved effectively via ARO. It is worth highlighting here that up to the authors' knowledge, the ARO algorithm is not utilized before in literature for tuning classical controllers.

B. ARO CONCEPT

The algorithm for ARO is developed from the nature of the survival strategies of rabbits. Rabbits have two main strategies to save their life, the first strategy is detour foraging, and the second is random hiding from enemies when they are attacked [57].

The detour foraging depends on the food types of rabbits that eat forbs, grass, and leafy weeds. To avoid the nest from being attacked by predators, rabbits do not feed the grass close to the nest holes but continually pursue foods far from their nests. Rabbits have a curiously widespread vision field, which depends on overhead scanning so they can discover foods over a wide area. The detour foraging strategy is considered exploration. This survival plan of rabbits is well known as the Chinese idiom says: ''rabbits do not eat the grass near its own nest''.

The second survival strategy of rabbits relies on a random hiding idea. As illustrated from the photo of Fig. 4, taken by Amethyst in [58], rabbits will grave many burrows around their nests to cheat enemies and to make the escape implementation easier, especially if they randomly choose one of the burrows as a shelter from predators. The bodybuilding of rabbits enables them to run fast as they have short forelegs and long back legs, strong muscles, and tendons. Moreover, rabbits can confuse their enemies by escaping in a zigzag motion, suddenly stopping while running, and sharp turning. The second strategy is considered exploitation.

The penalty of fast running is energy shrink, so rabbits need to adaptively switch between detour foraging and random hiding according to the energy.

C. ARO MATHEMATICAL MODEL

ARO hires the strategies of actual rabbits in foraging and hiding, along with their energy shrink foremost to transit between both strategies. The mathematical model of the ARO algorithm is divided into three main parts. Which are: detour foraging or exploration, random hiding or exploitation, and energy shrink constrain. The mathematical model is discussed in detail in [57].

1) DETOUR FORAGING (EXPLORATION)

In ARO, suppose that each rabbit in the group has its area with some grass and (d) burrows, and the rabbits randomly visit the position of each other for feeding. With foraging, rabbits are likely to confuse around a food source to eat sufficient food. Then, the ARO detour foraging behavior implies that each search individual tends to update its position towards the other search individual chosen randomly in the group and adds a perturbation.

FIGURE 4. Numerous burrows of the nest [58].

The detour foraging mathematical model of the rabbits is presented by:

$$\vec{v}_i(t+1) = \vec{x}_j(t) + R \cdot \left(\vec{x}_i(t) - \vec{x}_j(t)\right) + round\,(0.5 \cdot (0.05 + r_1)) \cdot n_1, \quad i, j = 1, \ldots, n \text{ and } j \neq i \tag{23}$$

$$R = L \cdot c \tag{24}$$

$$L = \left(e - e^{\left(\frac{t-1}{T}\right)^2}\right) \cdot \sin(2\pi r_2) \tag{25}$$

$$c(k) = \begin{cases} 1 & if\ k == g(l) \\ 0 & else \end{cases} \quad k = 1, \ldots, d \quad and\ l = 1, \ldots, \lceil r_3 \cdot d \rceil \tag{26}$$

$$g = rand\ perm\,(d) \tag{27}$$

$$n_1 \sim N(0, 1) \tag{28}$$

where $\vec{v}_i(t+1)$ is the candidate position of the i^{th} rabbit at the time t+1, $\vec{x}_j(t)$ is the position of the i^{th} rabbit at the time t, n is the size of a rabbit population, d is the dimension of the problem, T is the maximal number of iterations, $\lceil \cdot \rceil$ is the ceiling function, *round* indicates rounding to the nearest integer, *rand perm* returns a random permutation of the integers from 1 to d, r_1, r_2 and r_3 are three random numbers in the range of (0,1), l is the running length which represents the movement pace when performing the detour foraging, and n_1 is subject to the standard normal distribution.

Equation (23) shows that search individuals do a random search for foraging according to the position of others. This action permits a rabbit to transfer far away from its area to the area of the other rabbits. Especially a rabbit visiting others' nests instead of their nests significantly contributes to

exploration and guarantees the capability of the ARO algorithm to detect global search.

2) RANDOM HIDING (EXPLOITATION)

In ARO, at every iteration, a rabbit produces d burrows around it along each dimension of the search space randomly. It selects one of the burrows for hiding to decrease the probability of being attacked. The j^{th} burrow of the i^{th} rabbit is generated by:

$$\vec{b}_{i,j}(t) = \vec{x}_i(t) + H \cdot g \cdot \vec{x}_i(t), i = 1, \ldots, n \quad and\ j = 1, \ldots, d \tag{29}$$

$$H = \frac{T - t + 1}{T} \cdot r_4 \tag{30}$$

$$n_2 \sim N(0, 1) \tag{31}$$

$$g(k) = \begin{cases} 1 & if\ k == j \\ 0 & else \end{cases} k = 1, \ldots, d \tag{32}$$

From equation (29), the d burrows are created in the neighborhood of a rabbit along every dimension. H is the hiding parameter which is linearly decreased from 1 to $1/T$ with a random perturbation throughout iterations. According to this parameter, initially, these burrows are produced in a bigger neighborhood of a rabbit. As the iterations rise, this neighborhood gets reduced, too.

Rabbits randomly select a burrow from their burrows for shelter. To mathematically model this random hiding strategy, the following equations are applied:

$$\vec{v}_i(t+1) = \vec{x}_i(t) + R \cdot \left(r_4 \cdot \vec{b}_{i,r}(t) - \vec{x}_i(t)\right), i = 1, \ldots, n \tag{33}$$

$$g_r(k) = \begin{cases} 1 & if\ k == \lceil r_5 \cdot d \rceil \\ 0 & else \end{cases} k = 1, \ldots, d \tag{34}$$

$$\vec{b}_{i,r}(t) = \vec{x}_i(t) + H \cdot g_r \cdot \vec{x}_i(t) \tag{35}$$

where $\vec{b}_{i,r}(t)$ represents a randomly selected burrow for hiding from its d burrows, r_4 and r_5 are two random numbers in (0, 1).

From equation (33), the i^{th} search individual will try to update its position towards the randomly selected burrow from its d burrows. After one of both detour foraging and random hiding is achieved, the position update of the i^{th} rabbit is:

$$\vec{x}_i(t+1) = \begin{cases} \vec{x}_i(t) & f(\vec{x}_i(t)) \le f(\vec{v}_i(t+1)) \\ \vec{v}_i(t+1) & f(\vec{x}_i(t)) > f(\vec{v}_i(t+1)) \end{cases} \tag{36}$$

This equation signifies that if the fitness of the candidate position of the i^{th} rabbit is better than that of the current one, the rabbit will wildness the existing position and stay at the candidate position generated by either equation (23) or (33).

3) ENERGY SHRINK (SWITCH FROM EXPLORATION TO EXPLOITATION)

An energy factor is calculated to model the switch from exploration to exploitation. The energy factor in ARO is defined by the following formula, where r is the random number in (0,1):

$$A(t) = 4\left(1 - \frac{t}{T}\right) ln\frac{1}{r} \tag{37}$$

In ARO, when the energy factor $A(t) > 1$, a rabbit is disposed to randomly discover the areas of foraging for different rabbits in the exploration phase.

Then, the detour foraging occurs; when the energy factor $A(t) \le 1$, a rabbit is motivated to randomly exploit its burrows in the exploitation phase, therefore, the random hiding occurs.

Depending on the value of the energy factor A, ARO can change between either the detour foraging or random hiding. The energy factor A is decreased with the increase of iterations, which can strengthen each individual in the population to change between the detour foraging behavior and random hiding behavior. All the updates are efficiently realized until the termination criterion happens, and then the best solution is reimbursed. The pseudocode of ARO is described in Fig. 5.

- Randomly initialize a set of rabbits X_i (solutions) and evaluate their fitness Fit $_i$, so far X_{best} is the best-found solution.
- **While** the stop criterion is not satisfied, **For** each individual X_i, do the following:
- Calculate the energy factor A using equation (37).

If $A > 1$

- Choose a rabbit randomly from other individuals.
- Calculate R using equations (24)-(28).
- Perform detour foraging using equation (23).
- Calculate the fitness Fit $_i$.
- Update the position of the current individual using equation (36).

Else

- Generate d burrows and randomly pick one as hiding using equation (35).
- Perform random hiding using equation (33).
- Calculate the fitness Fit $_i$.
- Update the position of the individual using equation (36).

End If

- Update the best solution found so far, X_{best}.

End **For**
End **While**

- Return X_{best}

FIGURE 5. General procedures to apply the ARO algorithm.

V. RESULTS AND DISCUSSION

The studied IMG is simulated using the MATLAB environment, and the LFC system is thoroughly examined under various operational scenarios. The typical IMG shown in Fig. 1 is used to evaluate the suggested LFC scheme. The nominal values of the generating units and the system demand are listed in Table 1 [33]. Moreover, this IMG operates with

TABLE 1. Rated power of different sources in tested IMG.

Generator type	Rated power (kW)	MG base load (kW)
Diesel engine generators (DEG)	160	200
Fuel Cell (FC)	70	
Battery energy storage system (BESS)	30	
Photovoltaic system (PV)	30	
Wind Turbine (WT)	100	

TABLE 2. IMG parameters and time constants of different sources.

IMG	DEG	FC	BESS	PV
D (pu/Hz) = 0.015	$T1$=0.1	$T4$=0.26	$T7$=0.1	$T10$=12
$2H$=0.1667	$T2$=0.08	$T5$=0.04	$T8$=0.01	WT
R=2.4	$T3$=0.4	$T6$=0.004	$T9$=0.1	$T11$=2

parameters listed in Table 2 [38], a significant idea is to consider a specific amount of active power generated by the several DERs as a spinning reserve and a possible supply of active power for the LFC scheme.

In this section, the proposed multi-objective tuning method for different controllers of the LFC scheme is tested under different operational cases of IMG to prove its effectiveness. The optimization is accomplished for the case of 0.1 p.u step disturbance on the IMG, at 0 seconds, without the existence of RES. Simulations are carried out to study the frequency response considering $t_{sim} = 60$ s. The maximum iterations are chosen by 500, and the population size is 50 for this study.

The following suggested case studies will be extensively tested, where each case study has different load scenarios:

- First case study: load variations without RES availability.
- Second case study: load variations with the availability of RES.

A. THE EFFECTIVENESS OF ARO

At first, the performance of ARO is evaluated and compared with numerous recent optimization techniques applied in the literature for the LFC of IMG. The comparative study will include the optimization algorithms: genetic algorithm (GA), particle swarm optimization (PSO), GWO [30], WOA [31], MFO [29], MBA [27], and SMA [24].

The controllers of all controlled sources (DEG, BESS, and FC) are tuned based on the four popular error criteria: ISE, IAE, ITAE, and ITSE. Each distinct optimization algorithm has four runs that represent the four error criteria. For implementing a fair comparison among different optimization techniques, the cost function of all algorithms is equally evaluated with 100 iterations and a population size of 50. The IMG is subsequently subjected to a step load of 0.1 p.u at 0 sec, the optimal output gains of each algorithm are then applied to the controllers, and the objective functions are computed.

Table 3 displays the optimized values of these common error criteria for individual algorithms. As revealed, the ARO achieves better-optimized values than others in all single objective functions. So, as ARO has approved its trusted performance, the ARO algorithm will be applied to the proposed multi-objective optimization issue in this work in all the following scenarios for tested case studies.

B. TEST CASES AND TUNING OBJECTIVES

To distinguish the proficiency of the proposed multi-objective function, described in Section III, which consists of three objectives (J_1, J_2, & J_3), the authors will evaluate tuning the controller parameters of different controlled sources using the following formulations:

1. The first formulation is the single objective J_1 (optimal controller parameters are only based on ISE).
2. The second formulation is based on a multi-objective function which consists of two objectives by adding a control signal to ISE (J_1 & J_2).
3. The third formulation is based on a multi-objective function which consists of two objectives by the addition of the settling time to ISE (J_1 & J_3).
4. In the end, the proposed multi-objective formulation J which is based on J_1, J_2, & J_3.

Table 4 shows the optimally tuned gains of the four tested formulations for different sources' controllers. These optimal parameters will be applied to the system's controllers for investigating LFC. For providing a complete LFC analysis of the tested IMG, two case studies are proposed to test the system under different scenarios. The first case is with no availability of RES, while the second is with the availability of RES.

C. FIRST CASE STUDY WITH NO AVAILABILITY OF RES

In this investigated case study, the IMG is tested without the availability of RES, it is exposed to four different disturbances as follows:

1. Scenario 1: A step load of 0.1 and 0.15 p.u.
2. Scenario 2: A severe step load of 0.2 p.u.
3. Scenario 3: A multi-step load.
4. Scenario 4: A random load.

The well-known performance indices, ISE, the overshoot (OSH), the undershoot (USH), and Ts (the settling time) are assessed to evaluate and compare various tuning formulations. It is necessary to identify the priorities of each unique performance metric in the LFC problem to judge the various performances. The system operator determines the indices' significances based on the different MG operating conditions. The system's settling time presents the priest index in the LFC of IMG. Peak deviation at the time of load disturbance (USH in step-up load) is given as the second priority. Last but not least, OSH is taken into account to ensure system performance following the moment of disturbance.

1) SCENARIO 1 WITH STEP LOADS OF 0.1 P.U AND 0.15 P.U

This subsection establishes the effectiveness of the suggested multi-objective function for the IMG under two different step load disturbances of 0.1 and 0.15 p.u at t=1 s.

TABLE 3. Minimum objective functions obtained by different algorithms.

Single tuning criteria	Optimization technique							
	PSO	GA	MFO	MBA	WOA	GWO	SMA	**ARO**
IAE	0.060079	0.058896	0.051717	0.059045	0.058207	0.054405	0.051542	**0.051277**
ITAE	0.592883	0.65264	0.53868	0.564676	0.610396	0.549339	0.552996	**0.534740**
ITSE	0.043728	0.044784	0.044402	0.04397	0.044814	0.043585	0.043593	**0.043558**
ISE	0.004236	0.004316	0.004326	0.004256	0.004356	0.004235	0.004326	**0.004217**

TABLE 4. Optimum controllers' parameters for different sources.

Objective function	Optimal controller parameter of controlled sources							
	PID for DEG			PI for BESS		PID for FC		
	K_p	K_i	K_d	K_p	K_i	K_p	K_i	K_d
J_1	0.6378	0.2709	0.3631	0.5603	0.0609	0.6451	1.9669	0.2516
J_1 & J_2	0.4772	0.6756	0.2115	0.4562	0.6618	0.7149	0.6754	0.1537
J_1 & J_3	0.7205	0.3992	0.3531	0.5362	0.1996	0.5854	1.6421	0.2334
Proposed formulation J (J_1, J_2, & J_3)	0.5434	0.6770	0.2022	0.4695	0.6622	0.6259	0.6792	0.1918

Figure 6-a illustrates the system's change in frequency (ΔF) in response to the step load perturbation of 0.1 p.u delivered at t = 1 s. Table 5 offers the performance indices for various tuning formulations. Since all controllers consider sources' GRC, Table 5 indicates that all objectives have the same USH; hence, the formulation with the lowest OSH will settle faster. According to Fig. 6-a and Table 5, the proposed multi-objective formulation J delivers the fastest reaction with 0.0133 p.u overshoot. Using the multi-objective formulation J, Ts and OSH are improved by 45.16 and 21.2%, respectively. The system settles in 2.96 s, compared to 5.4 s of the single objective J_1.

It is vital to notice that including Ts in the second formulation of the multi-objective (J_1 & J_3) directly improves Ts, but it has the penalty of high control action. It results in a larger OSH of 0.0226 p.u and a slower response than the proposed formulation J with $Ts = 4.03$ s. The formulation of J_1 and J_2 may adopt the system OSH after disturbance's instant to be lower than the formulation of J_1 & J_3 with OSH of 0.0145 p.u, and the settling is faster at 3.37 s by adding the control signal in the objective function. On the other hand, the proposed multi-objective formulation J loses disregarded undershoot percent and tiny ISE percent w.r.t. the single objective J_1 by -0.14 % and -4.43 %, respectively.

When the IMG undergoes 0.15 p.u step disturbance at t=1 s, the proposed multi-objective formulation J was superior to the others as shown in Fig. 6-b. Table 6 displays the proposed tuning objective performance indices w.r.t others. It settled in 3.8 s with a 15.73% improvement over J_1. Despite tuning the controller's parameters based on J_1 (ISE), they failed to achieve minimum ISE in this scenario. The proposed multi-objective formulation J has an ISE of 0.01941, while J_1's was 0.02623. The proposed multi-objective formulation J reduces the system's OSH to 0.1054 p.u and improves it by 25.39 %.

Scenario 1, under the two different step load disturbances, reveals how a faster system's settlement with less overshoot is achieved by using the proposed multi-objective formulation J and the formulation (J_1 & J_2) that take into account control signals. On the other hand, a slower system settlement and more overshoots would result from using the formulations that neglect the control signals during the tuning, such as the single objective J_1 or the multi-objective formulation of J_1 & J_3.

2) SCENARIO 2 WITH A SEVERE STEP CHANGE OF 0.2 P.U

The key purpose of this scenario is to examine the robustness of the proposed multi-objective formulation J when the system is exposed to a severe step disturbance of 0.2 p.u w.r.t other formulations. Whether the system responds faster and keeps improving or not is the main issue here.

According to Fig. 7, even after subjecting the system to a severe step of 0.2 p.u at t = 1 s, the proposed multi-objective formulation J and (J_1 & J_2) maintained system stability. They successfully managed the sudden and severe load by limiting the control signals to specific controllers, delivering the right amount of power, and guaranteeing system stability. In contrast, the other tuning objectives J_1 and (J_1 & J_3) failed to preserve the system's stability. They will subject the tuned controllers to high control signals for the controlled sources, making them unable to react sensibly enough to keep the system stable. Moreover, the objective (J_1 & J_3) generates more control actions than objective J_1, so undershoots and overshoots occur later for objective (J_1 & J_3) compared with objective J_1.

3) SCENARIO 3 WITH A MULTI-STEP LOAD

In this scenario, the IMG is exposed to multi-step disturbances have maxima and minima values of 0.075 p.u and

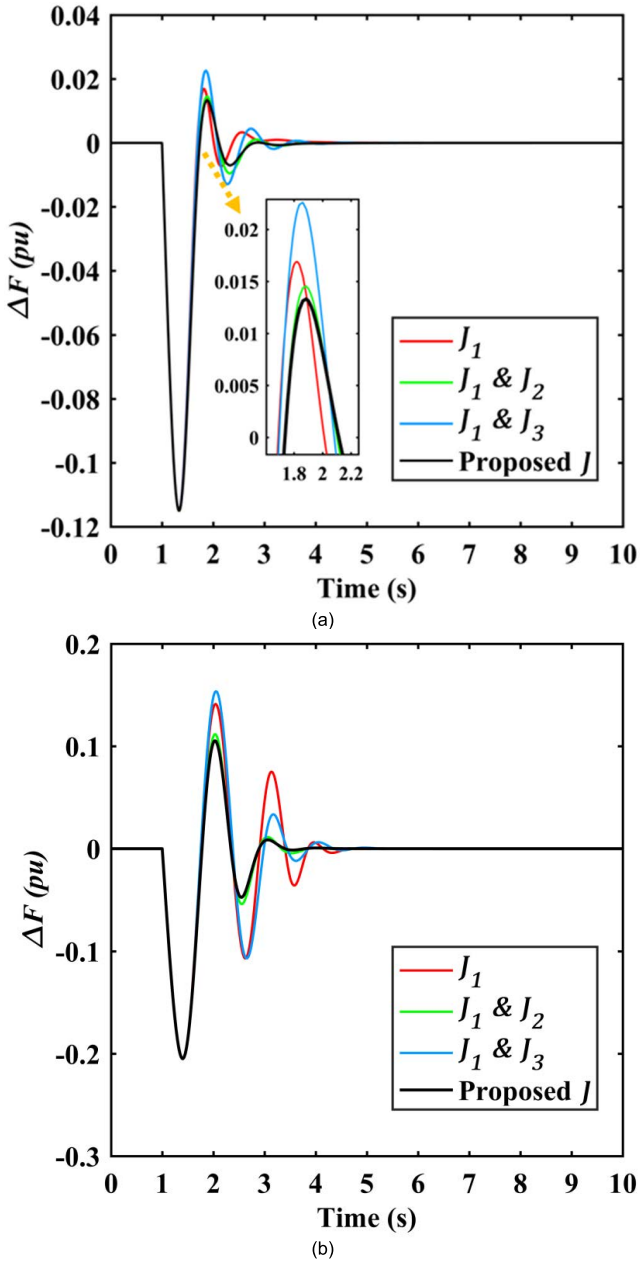

FIGURE 6. Frequency deviations of the tested IMG for different tuning objectives in Scenario 1. (a) a step load of 0.1 p.u at t=1 s, and (b) a step load of 0.15 p.u at t=1 s.

−0.075 p.u, respectively, while the time difference between two successive steps is 5 s as illustrated in Fig. 8. The IMG will have two repetitive states. The first state is over-frequency when the load steps down from 0.075 p.u to −0.075 p.u (e.g., at t=5 s). The second state is under-frequency when the load steps up from −0.075 p.u to 0.075 p.u (e.g., at t=10 s). Thus, it is essential to ensure that the controllers' tuned parameters have enabled the system to settle before the next disturbance.

The performance analysis is then complete. Consequently, various tuning objectives' system responses are evaluated in Fig. 9 indicating the system responses following the over-frequency and under-frequency states, respectively. As previously discussed in Scenario 1, the peaks during the instants of disturbances initiation will be excluded from comparison since they are nearly identical. As displayed in Fig. 9, the proposed multi-objective formulation J for parameters tuning has a superior response to other formulations.

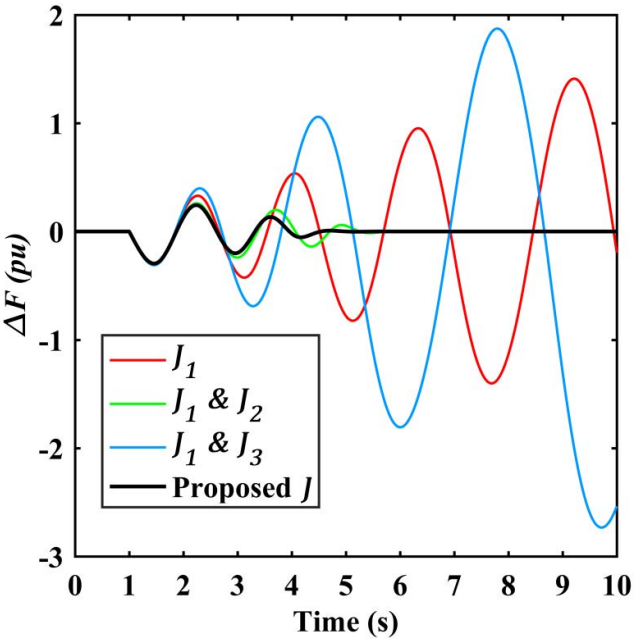

FIGURE 7. Frequency deviations of the tested IMG for different tuning objectives in Scenario 2 with a severe step load of 0.2 p.u at t=1 s.

Table 7 summarizes the performance indices for such multi-step disturbance (two states of over-frequency at t=5 s, and under-frequency at t=10 s), which are the settling time, the first peak following the instant of disturbance, and the decay ratio (DR) index. It is worth noting that the DR index is a good measure of how rapidly the oscillations are decreasing. The lower DR, the rapid decay oscillation until the system settles.

The proposed multi-objective formulation J has superiority for all estimated indices over others. It could enable the system to settle with minimum times either in over or under-frequency states. The system has a minimum 1st peak in two states (1st USH and 1st OSH of over and under-frequency states after step instant) of −0.1056 p.u and 0.1048 p.u, respectively. So, it can provide the minimum setting times of 3.75 s for the over-frequency state and 3.8 s for the under-frequency state.

On the other hand, the single objective J_1 and the multi-objective formulation of (J_1 & J_3) provide higher control signals to different sources which significantly help the system to settle close to the time difference limit (5 seconds).

TABLE 5. Performance indices and improvement percentage in Scenario 1 with a step load of 0.1 p.u at t=1 s.

Objective function	Performance indices				% Improvement w.r.t J_1			
	ISE	OSH	USH	Ts	ISE	OSH	USH	Ts
J_1	0.00422	0.0169	-0.11485	5.40	-	-	-	-
J_1 & J_2	0.00441	0.0145	-0.11505	3.37	-4.58	13.97	-0.17	37.55
J_1 & J_3	0.00436	0.0226	-0.11491	4.03	-3.48	-33.81	-0.05	25.50
Proposed formulation J (J_1, J_2, & J_3)	0.00440	**0.0133**	-0.11501	**2.96**	-4.43	**21.20**	-0.14	**45.16**

TABLE 6. Performance indices and improvement percentage in Scenario 1 with a step load of 0.15 p.u at t=1 s.

Objective function	Performance indices				% Improvement w.r.t J_1			
	ISE	OSH	USH	Ts	ISE	OSH	USH	Ts
J_1	0.02623	0.1412	-0.204974	4.51	-	-	-	-
J_1 & J_2	0.01999	0.1117	-0.205000	3.86	23.79	20.89	-0.013	14.57
J_1 & J_3	0.02654	0.1537	-0.204989	4.59	-1.18	-8.81	-0.007	-1.77
Proposed formulation J (J_1, J_2, & J_3)	**0.01941**	**0.1054**	**-0.204986**	**3.80**	**25.98**	**25.39**	**-0.006**	**15.73**

TABLE 7. Performance indices in Scenario-3 (a multi-step load).

Objective function	Over-frequency (t= [5-10 s])			Under-frequency (t= [10-15 s])		
	1st USH	TS	% DR	1st OSH	TS	% DR
J_1	-0.1446	4.82	59.24	0.1427	4.72	54.15
J_1 & J_2	-0.1105	3.86	19.87	0.1107	3.85	20.38
J_1 & J_3	-0.1531	4.61	39.39	0.1521	4.59	38.76
Proposed formulation J (J_1, J_2, & J_3)	**-0.1056**	**3.75**	**17.80**	**0.1048**	**3.80**	**18.45**

In the over-frequency condition, the system settles in 4.82 s and 4.61 s, respectively, while in the under-frequency state, it takes 4.72 s and 4.59 s, respectively.

The other multi-objective formulation of (J_1 & J_2) has achieved very well performances and enabled the system to settle in times almost equal to the proposed multi-objective formulation J of 3.85 s and 3.86 s, respectively.

DR index is estimated in Table 7 to indicate how quickly the oscillations are diminishing. As illustrated, the proposed multi-objective formulation J has the lowest DR values in the over-frequency and under-frequency states of 17.8 % and 18.45 %, respectively. Besides, the formulation (J_1 & J_2) could provide a very satisfactory value for DR of 19.87 % in the over-frequency condition and 20.83 % in the under-frequency state when the tuning process considers the control signals. Recalling the penalty of higher control actions will be for objectives that do not consider control signals in the tuning procedure, such as the single objective J_1 and multi-objective formulation (J_1 & J_3). They offered a terrible DR (high values) of 59.24 % and 39.39 % for the over-frequency state and 54.15 % and 38.76 % for the under-frequency state.

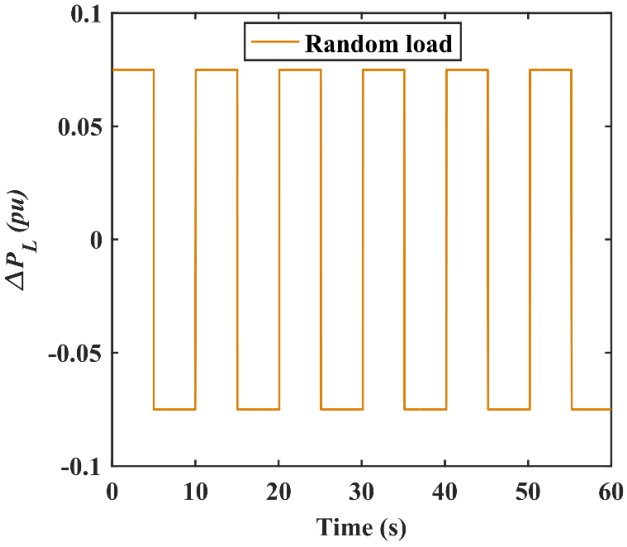

FIGURE 8. A multi-step disturbance of Scenario 3.

4) SCENARIO 4 WITH A RANDOM LOAD

In this scenario, the tested IMG is examined for severe random load conditions, as given in Fig. 10, using the block of band-limited white noise that generates normally distributed random numbers.

Figure 11 displays the variations in frequency for the different investigated four objectives for parameters' tuning in this scenario of a random load. Due to the reduced inertia in

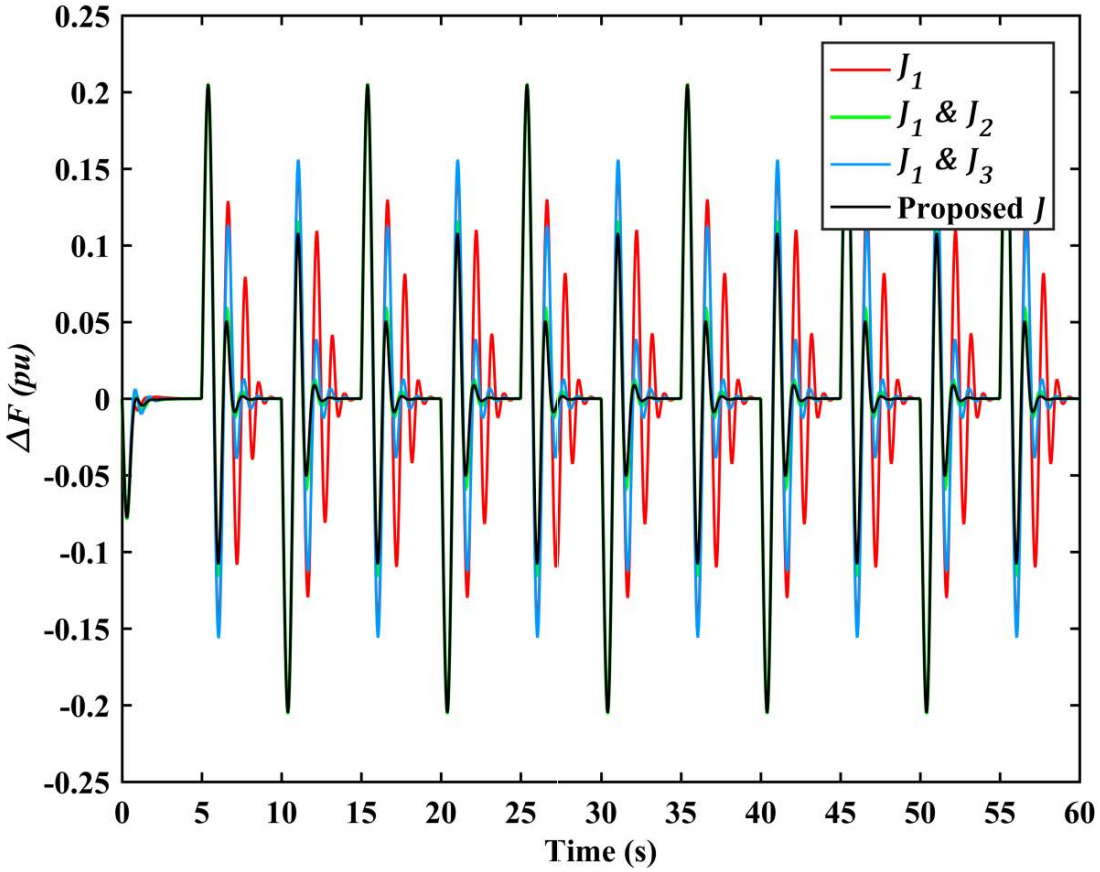

FIGURE 9. Frequency deviations of the tested IMG for different tuning objectives in Scenario 3 with multi-step load changes every 5 seconds.

the system, the frequency oscillates with a larger amplitude of frequency. As the system is very sensitive to random load, it may not have any fast-responding standby to suppress the variations in frequency, which may result in system instability.

As shown, all objectives respond well till 30 seconds. The zoom region in Fig. 11 ensures that the tuned parameters based on the proposed multi-objective formulation J have the lowest frequency variations at high spikes of the random load (dashed circles in the zoom region in Fig. 11).

As shown, both the proposed multi-objective formulation J and the formulation (J_1 & J_2), considering the control signals in the tuning process, could maintain the system stability when the system is subjected to severe value random load after t=30 s, in contrast to the other tuning objectives which fail in preserving the system stability. Indeed, they behaved sensibly to fast oscillations of the random load by limiting the control signals for different controllers to supply sufficient power and keep the system stable.

On the contrary, the other objectives (single objective J_1 and multi-objective formulation (J_1 & J_3) will be subject to large control signals for various controlled sources and thus fail to respond fast during random load oscillations. Therefore, when the system is exposed to that severe random load, it cannot maintain system stability after t=30 s.

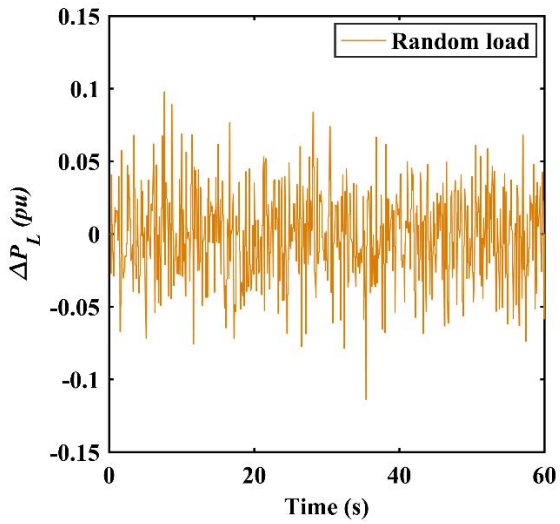

FIGURE 10. Random load in Scenario 4.

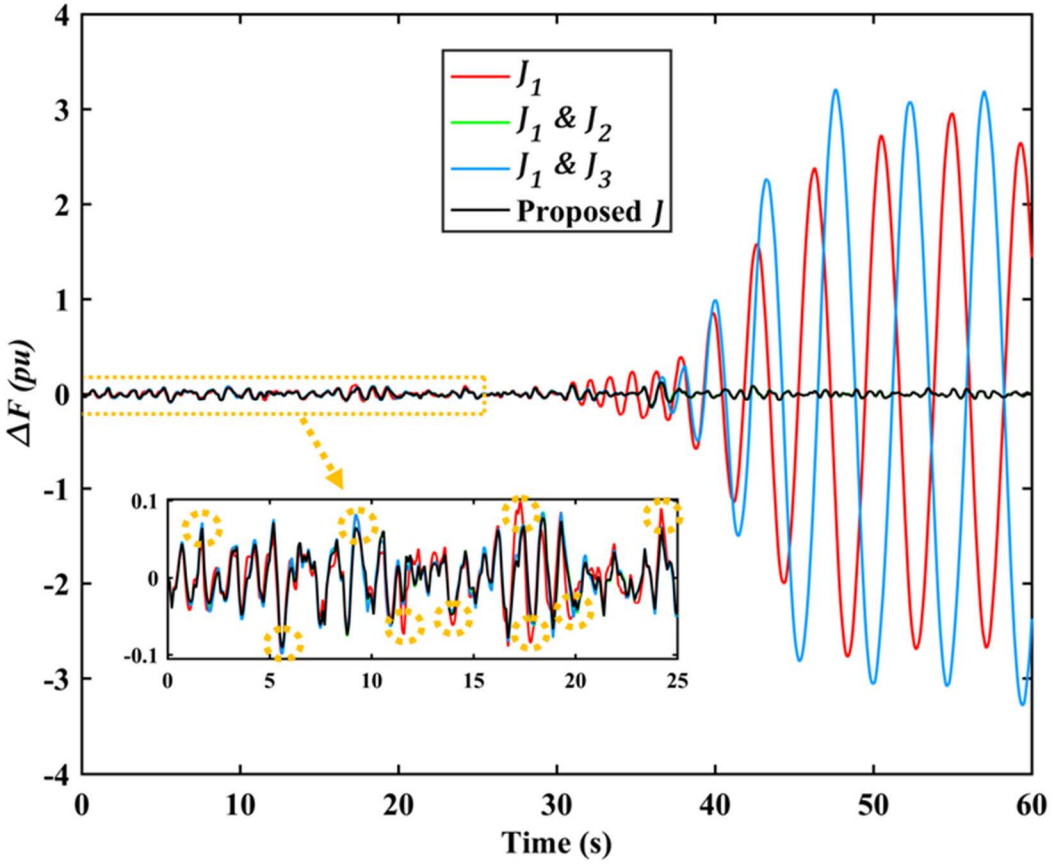

FIGURE 11. Frequency deviations of the tested IMG for different tuning objectives in Scenario 4 with a random load.

D. SECOND CASE STUDY WITH AVAILABILITY OF RES

For this case study, the IMG is tested under different scenarios with RES availability (PV and wind). As shown in Fig. 12, the RESs freely supply all their available power to the IMG, while the DEG, BESS, and FC sources change their power output based on system frequency fluctuations.

RES has two distinctive impacts on the IMG's frequency. The first effect is the over-frequency when RESs supply excessive power to the IMG (e.g., at t=30 s in Fig. 12), and the second effect is the under-frequency which occurs when their available power decreases according to the weather conditions (e.g., at t=50 s in Fig. 12).

The tested scenarios will be as follows:

1. PV and WT systems are added to the tested IMG without load disturbances.
2. A multi-step load is subject to the system in addition to the availability of RES.
3. A step load is applied with the critical excessive power of RES.
4. A step load is applied with the critical shortage power of RES.

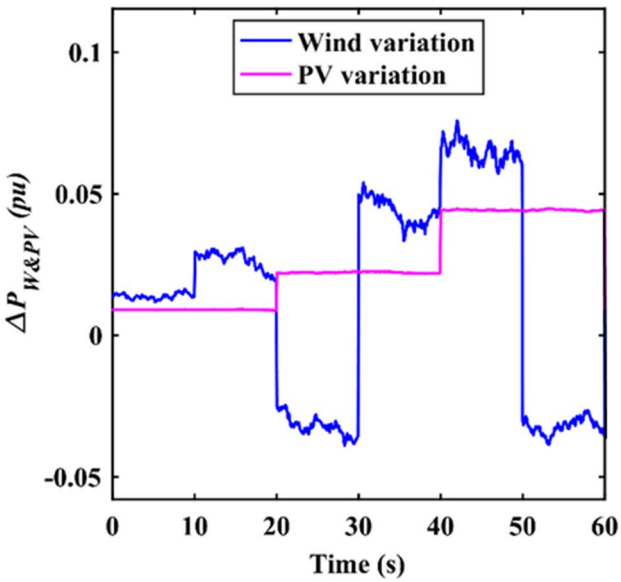

FIGURE 12. RESs variations.

1) SCENARIO 1 WITH RESs INCLUDED WITHOUT LOAD VARIATIONS

The variations in frequency are studied in this scenario as demonstrated in Fig. 13 when adding RESs

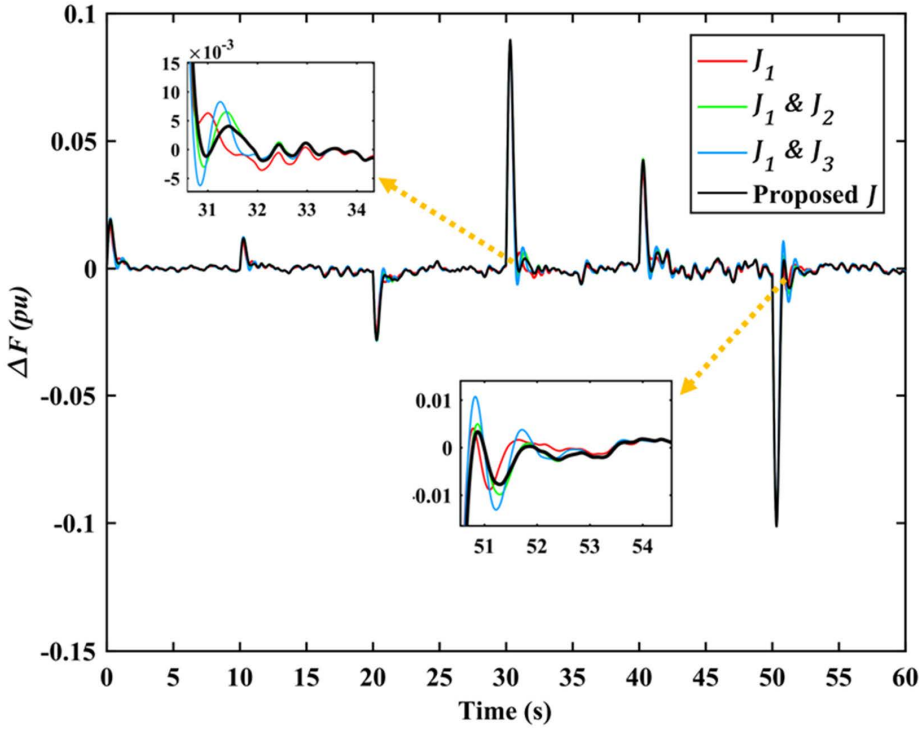

FIGURE 13. Frequency deviations of the tested IMG when adding RES with the absence of load variations (scenario 1).

without any load variation to check the robustness of different tuning objectives to enhance the system stability.

As illustrated in Fig. 13, all objectives can enhance the system stability along different variations of RES. But for the high variations shown in the zoom areas of Fig. 13 (upper, down), the proposed multi-objective tuning formulation J is preferred over other alternatives because it settles more quickly and makes sense to assign control actions to various controllers.

Additionally, the formulation (J_1 & J_2) can perform better than the single objective and the formulation (J_1 & J_3) in larger RES swings. It is clear that the formulations depend on limiting control actions, like the proposed multi-objective tuning formulation J, and the formulation (J_1 & J_2) can perform better than the others in critically high RES variations and deliver acceptable responses in small RES fluctuations.

2) SCENARIO 2 WITH RESs INCLUDED AND A MULTI-STEP LOAD

A periodic multi-step load is applied in this scenario every 15 s. It has maxima and minima of 0.075 p.u and −0.075 p.u, respectively. The system's frequency responses are displayed in Fig. 14. The system exhibits repeated critical over-frequency (e.g., at t=15 and 45 s) because the load is reduced by 0.15 p.u with only a little increase in RES power. Critical under-frequency (e.g., at t=30 s) occurs because the load is increased by 0.15 p.u with the shortage in RES power.

The multi-objective tuning formulation J that was proposed for tuning parameters has the ability to sensibly limit the control signals of multiple controllers, thereby ensuring low overshoots and undershoots after the instant of the disturbance. As a consequence, it has the benefit of being able to settle any violations in the system frequency faster than other formulations, regardless of whether the fluctuations were significant or minor.

3) SCENARIO 3 WITH A STEP-DOWN LOAD AND EXCESSIVE RESs' POWER

As revealed in Fig. 13, the first critical variation in the system frequency due to adding RESs sources arises at t=30 s, which presents the critical over-frequency state as the available RESs power is excessive. In this scenario, it is supposed to apply a step-down load at that critical instant to maximize the over-frequency problem. A step-down load of −0.1 p.u is applied at t=30 s to study the system stability.

As seen in Fig. 15, a decrease in load and the availability of surplus power from RES may cause the system's critical over-frequency to occur, which may cause instability. The proposed multi-objective formulation J and the formulations (J_1 & J_2) are superior as they preserve system stability. On the contrary, the single-objective

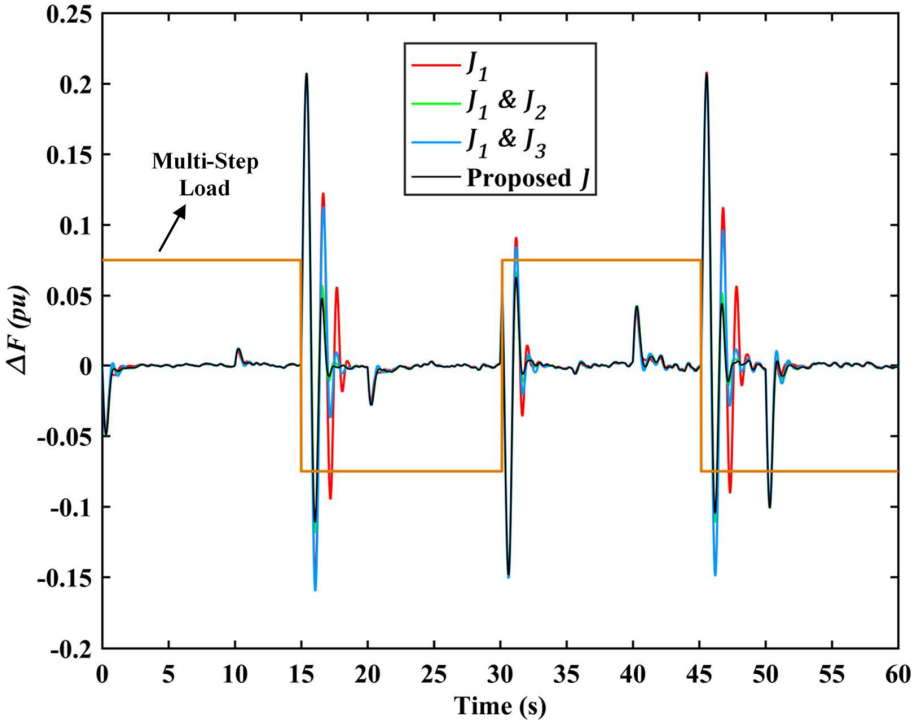

FIGURE 14. Frequency deviations of the tested IMG when multi-steps are applied to the system with the availability of RES (Scenario 2).

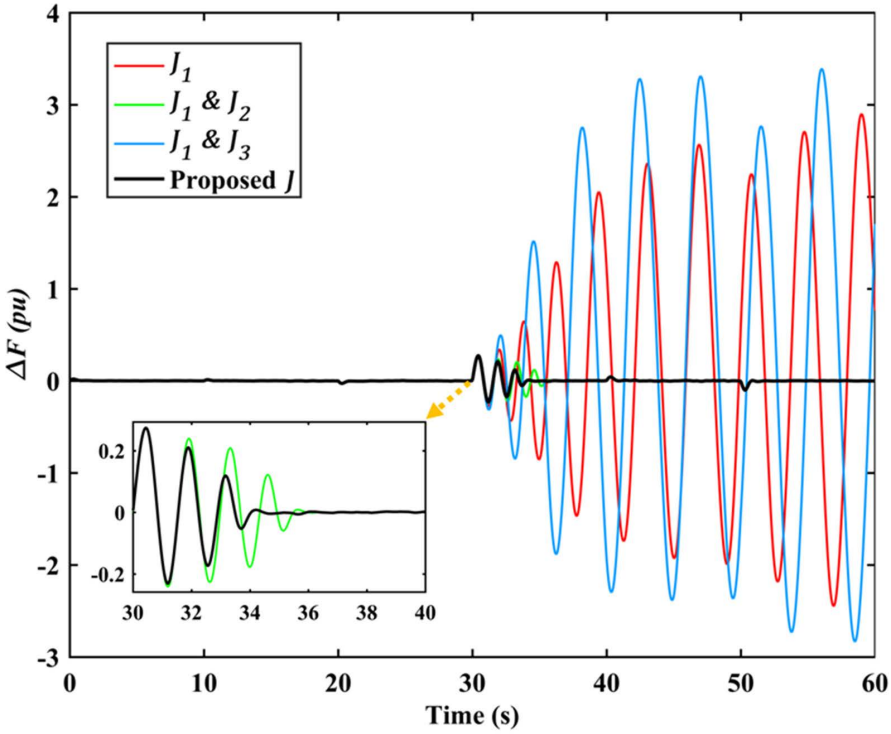

FIGURE 15. Frequency deviations of the tested IMG tuned based on different objectives in Scenario 3 with the availability of RESs' excessive power.

formulation J_1 and (J_1 & J_3) that neglect control signals during the tuning process are unable to respond appropriately because of their enlarged control actions, which causes system instability.

Moreover, the proposed objective has provided little more improvement in the overall performance than the formulation (J_1 & J_2), which does not consider the settling time as shown in the lower zoom area of Fig. 15.

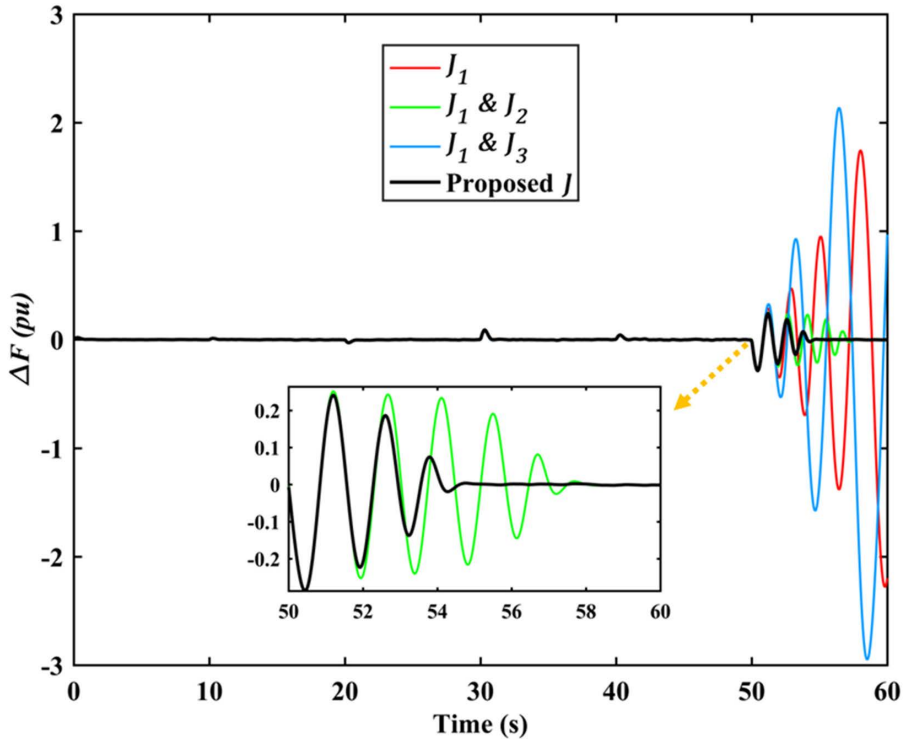

FIGURE 16. Frequency deviations of the tested IMG tuned based on different objectives in Scenario 4 with the shortage of RESs' power.

4) SCENARIO 4 WITH A STEP-UP LOAD AND SHORTAGE OF RESs' POWER

This scenario is investigated to evaluate the stability of IMG has RES and a step-up load of 0.1 p.u is applied at t=50 s. It is assumed to maximize the critical under-frequency proposed by RESs due to their shortage in available power at the instant of t=50 s, as demonstrated previously in Fig. 13.

Again, as shown in Fig. 16, the tuned parameters based on the single objective J_1 and the formulation of (J_1 & J_3) can not preserve the frequency stability at the instant for applying the step-up disturbance at t=50 s. In contrast, the tuned parameters based on the proposed multi-objective formulation can keep the system stable after the step-up disturbance at t=50s, besides providing better performance than the formulation (J_1 & J_2).

VI. SENSITIVITY ANALYSIS (SYSTEM PARAMETERS' UNCERTAINTY)

A comprehensive sensitivity analysis is performed to evaluate how the system responds to a step change while the system parameters vary by a margin of ±25% from their nominal values. There are two distinct ways to alter the system's parameters. The first includes varying one of the following separately: the system's inertia, damping coefficient, speed regulation constant, or sources' time constants. Second, all system parameters are changed at once.

For the first way, Fig. 17 illustrates the system frequency response of controllers tuned based on the proposed multi-objectives with the individual variation of system parameters such as inertia constant (H), damping coefficient (D), speed regulation constant (R), and sources time constants. The suggested LFC system responds well to the variations in H, as seen in Fig. 17-b, and stabilizes rather closely to the scenario with nominal parameters. The suggested LFC technique would successfully stabilize the system for H fluctuations of −25% in less than 1 s after the case of nominal parameters has stabilized. As demonstrated in Fig. 17-b and Fig. 17-c, peak OSH, and USH are quite similar. It reveals how well the system adapts to variations in R and D and how it is capable of settling simultaneously. No matter what adjustments are made to the time constants of the sources as shown in Fig.17-d, the system response does not cause any considerable differences in the settling time compared to the nominal case. The peak OSH and USH also closely approximate one another.

For the second way, Fig. 18 displays how the suggested LFC scheme behaves when the system's parameters are altered by ±25% at once. As can be observed, changing the system's parameters by a value of −25% would result in a noticeable change in how it responds. Even yet, the established LFC technique has the capacity to stabilize the system and settle it in less than two seconds after the nominal case has been settled. Moreover, the system's behavior differs slightly depending on a +25% change in system parameters related to the situation of nominal parameters.

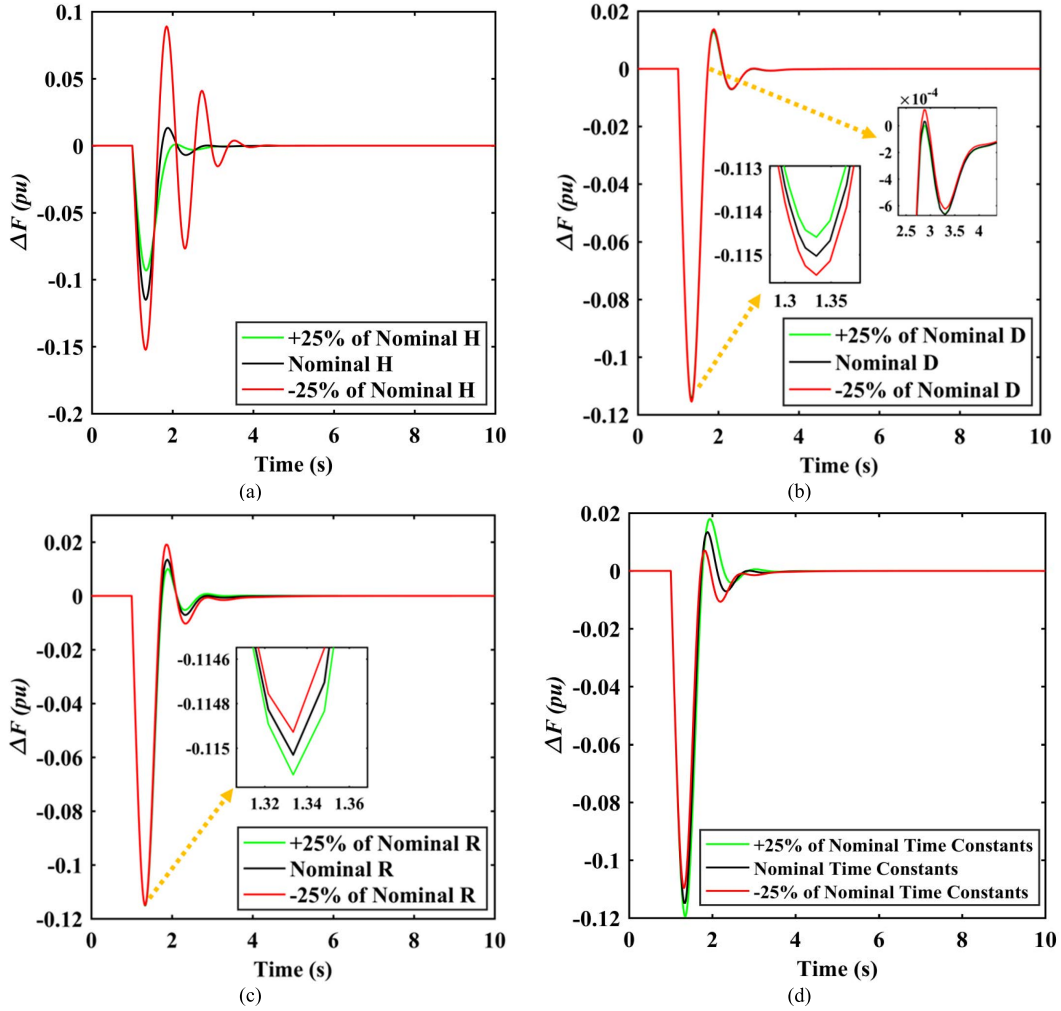

FIGURE 17. Frequency deviations of the tested IMG for different tuning objectives in case of changing the system parameters separately.

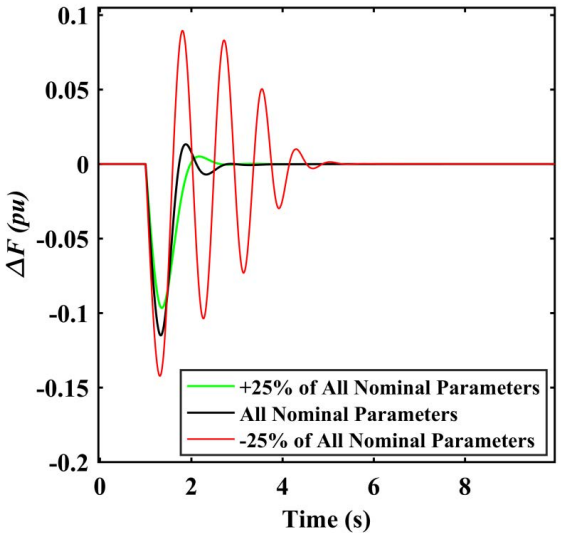

FIGURE 18. Frequency deviations of the tested IMG for different tuning objectives in case of the system parameters are changed at once.

VII. CONCLUSION

A novel multi-objective tuning approach is introduced to optimize IMG's LFC's traditional PI and PID controller parameters. The proposed multi-objective tuning uses controller control signals, settling time, and the integral square of frequency deviation to determine the optimal gains of various controllers used in the LFC scheme of a low inertia IMG. It considers anti-windup and practical generation rate limits for different sources.

At first, the recent ARO algorithm has approved its superiority among several optimization algorithms based on the conventional single-criterion tuning formulations: ISE, IAE, ITAE, and ITSE. Consequently, the proposed multi-objective formulation is applied based on ARO to tune the controllers.

For distinct IMG operating scenarios, the proposed multi-objective formulation for controller tuning is extensively compared to three others. The three formulations were ISE-based single tuning, ISE with control signals

coming from different controllers, and ISE with settling time. The frequency stability of the IMG is evaluated in two extensive case studies, one without RES and one with RES.

In the absence of RES, the IMG is tested under four load scenarios: a step, a severe step disturbance, a multi-step, and a severe random disturbance. ISE, OSH, USH, and settling time performance indicators are assessed to examine frequency responses.

- The proposed tuning approach outperformed other tuning formulas in OSH and the settling time under a 0.1 p.u step disturbance.
- It enhanced all performance metrics with a high step disturbance of 0.15 p.u.
- It provided the best settling time and fastest decay oscillations for periodic multi-step disturbances.
- It could maintain system stability for the severe step of 0.2 p.u and random disturbances, unlike those that do not consider control signals.

In the presence of RES, IMG stability is tested under four scenarios: no load disturbance, multi-step, step-up, and step-down disturbances.

- In the first and second scenarios, the proposed multi-objective tuning was better than other tuning objectives for both small and large fluctuations.
- During critical RES excess and shortage, the third and fourth scenarios use step-up and step-down disturbances. The proposed multi-objective formulation preserved system stability. On the contrary, the formulations that neglect control signals during tuning cannot respond effectively, resulting in system instability

Finally, sensitivity analyses of the proposed LFC technique are carried out for $\pm 25\%$ system parameter change. The suggested multi-objective formulation keeps the system stable when system parameters change.

Notably, future research will investigate the viability of integrating the proposed multi-objective tuning in more sophisticated controllers like fractional-order PID and cascaded loop controllers.

REFERENCES

[1] N. W. A. Lidula and A. D. Rajapakse, "Microgrids research: A review of experimental microgrids and test systems," *Renew. Sustain. Energy Rev.*, vol. 15, no. 1, pp. 186–202, 2011, doi: 10.1016/j.rser.2010.09.041.

[2] T. Kerdphol, F. S. Rahman, Y. Mitani, M. Watanabe, and S. Küfeoğlu, "Robust virtual inertia control of an islanded microgrid considering high penetration of renewable energy," *IEEE Access*, vol. 6, pp. 625–636, 2018, doi: 10.1109/ACCESS.2017.2773486.

[3] R. Aazami, O. Heydari, J. Tavoosi, M. Shirkhani, A. Mohammadzadeh, and A. Mosavi, "Optimal control of an energy-storage system in a microgrid for reducing wind-power fluctuations," *Sustainability*, vol. 14, no. 10, pp. 6183–6197, 2022, doi: 10.3390/su14106183.

[4] M. S. Guney and Y. Tepe, "Classification and assessment of energy storage systems," *Renew. Sustain. Energy Rev.*, vol. 75, pp. 1187–1197, Aug. 2017, doi: 10.1016/j.rser.2016.11.102.

[5] F. Zhang, Z. Hu, X. Xie, J. Zhang, and Y. Song, "Assessment of the effectiveness of energy storage resources in the frequency regulation of a single-area power system," *IEEE Trans. Power Syst.*, vol. 32, no. 5, pp. 3373–3380, Sep. 2017, doi: 10.1109/TPWRS.2017.2649579.

[6] A. Chauhan and R. P. Saini, "A review on integrated renewable energy system based power generation for stand-alone applications: Configurations, storage options, sizing methodologies and control," *Renew. Sustain. Energy Rev.*, vol. 38, pp. 99–120, Oct. 2014, doi: 10.1016/j.rser.2014.05.079.

[7] J. J. Justo, F. Mwasilu, J. Lee, and J.-W. Jung, "AC-microgrids versus DC-microgrids with distributed energy resources: A review," *Renew. Sustain. Energy Rev.*, vol. 24, pp. 387–405, Aug. 2013, doi: 10.1016/j.rser.2013.03.067.

[8] M. R. Khalghani, M. H. Khooban, E. Mahboubi-Moghaddam, N. Vafamand, and M. Goodarzi, "A self-tuning load frequency control strategy for microgrids: Human brain emotional learning," *Int. J. Electr. Power Energy Syst.*, vol. 75, pp. 311–319, Feb. 2016, doi: 10.1016/j.ijepes.2015.08.026.

[9] M. Yuan, Y. Fu, Y. Mi, Z. Li, and C. Wang, "The coordinated control of wind-diesel hybrid micro-grid based on sliding mode method and load estimation," *IEEE Access*, vol. 6, pp. 76867–76875, 2018, doi: 10.1109/ACCESS.2018.2883492.

[10] B. Wu, Y. Lang, N. Zargari, and S. Kouro, *Power Conversion and Control of Wind Energy Systems*. New York, NY, USA: Wiley, 2011.

[11] L. A. de Souza Ribeiro, O. R. Saavedra, S. L. de Lima, and J. G. de Matos, "Isolated micro-grids with renewable hybrid generation: The case of Lençóis island," *IEEE Trans. Sustain. Energy*, vol. 22, no. 1, pp. 1–11, Jan. 2010, doi: 10.1109/TSTE.2010.2073723.

[12] E. Mojica-Nava, C. A. Macana, and Y. Quijano, "Dynamic population games for optimal dispatch on hierarchical microgrid control," *IEEE Trans. Syst., Man, Cybern., Syst.*, vol. 44, no. 3, pp. 306–317, Mar. 2014, doi: 10.1109/TSMCC.2013.2266117.

[13] M. Hosseinzadeh and R. Salmasi, "Robust optimal power management system for a hybrid AC/DC micro-grid," *IEEE Trans. Sustain. Energy*, vol. 6, no. 3, pp. 675–687, Oct. 2015, doi: 10.1109/TSTE.2015.2405935.

[14] Y. V. Hote and S. Jain, "PID controller design for load frequency control: Past, present and future challenges," *IFAC-PapersOnLine*, vol. 51, no. 4, pp. 604–609, 2018, doi: 10.1016/j.ifacol.2018.06.162.

[15] D. Izci, S. Ekinci, and S. Mirjalili, "Optimal PID plus second-order derivative controller design for AVR system using a modified Runge Kutta optimizer and Bode's ideal reference model," *Int. J. Dyn. Control*, pp. 1–18, Oct. 2022, doi: 10.1007/s40435-022-01046-9.

[16] S. Ekinci, D. Izci, and M. Kayri, "An effective controller design approach for magnetic levitation system using novel improved manta ray foraging optimization," *Arabian J. Sci. Eng.*, vol. 47, no. 8, pp. 9673–9694, Aug. 2022, doi: 10.1007/s13369-021-06321-z.

[17] Y.-H. Moon, H.-S. Ryu, J.-G. Lee, K.-B. Song, and M.-C. Shin, "Extended integral control for load frequency control with the consideration of generation-rate constraints," *Int. J. Electr. Power Energy Syst.*, vol. 24, no. 4, pp. 263–269, 2002, doi: 10.1016/S0142-0615(01)00036-9.

[18] S. Velusami and I. A. Chidambaram, "Design of decentralized biased dual mode controllers for load–frequency control of interconnected power systems," *Electr. Power Compon. Syst.*, vol. 34, no. 10, pp. 1057–1075, Oct. 2006, doi: 10.1080/15325000600630327.

[19] K. R. Sudha and R. V. Santhi, "Robust decentralized load frequency control of interconnected power system with generation rate constraint using type-2 fuzzy approach," *Int. J. Electr. Power Energy Syst.*, vol. 33, no. 3, pp. 699–707, Mar. 2011, doi: 10.1016/j.ijepes.2010.12.027.

[20] J. Öhr, "Anti-windup and control of systems with multipleinput saturations: Tools, solutions and case studies," Ph.D. dissertation, Dept. Elect. Eng. With Specialization Autom. Control, Uppsala Univ., Uppsala, Sweden, 2003.

[21] C. Huang, D. Yue, X. Xie, and J. Xie, "Anti-windup load frequency controller design for multi-area power system with generation rate constraint," *Energies*, vol. 9, no. 5, p. 330, Apr. 2016, doi: 10.3390/en9050330.

[22] D. İzci and S. Ekinci, "Comparative performance analysis of slime mould algorithm for efficient design of proportional–integral–derivative controller," *Electrica*, vol. 21, no. 1, pp. 151–159, 2021, doi: 10.5152/ELECTRICA.2021.20077.

[23] S. Ekinci, D. Izci, E. Eker, and L. Abualigah, "An effective control design approach based on novel enhanced Aquila optimizer for automatic voltage regulator," *Artif. Intell. Rev.*, pp. 1–32, Jun. 2022, doi: 10.1007/s10462-022-10216-2.

[24] M. Khamies, G. Magdy, S. Kamel, and S. K. Elsayed, "Slime mould algorithm for frequency controller design of a two-area thermal-PV power system," in *Proc. IEEE Int. Conf. Autom. Congr. Chilean Assoc. Autom. Control*, Valparaíso, Chile, Mar. 2021, pp. 1–7, doi: 10.1109/ICAACCA51523.2021.9465183.

[25] Y. Xu, C. Li, Z. Wang, N. Zhang, and B. Peng, "Load frequency control of a novel renewable energy integrated micro-grid containing pumped hydropower energy storage," *IEEE Access*, vol. 6, pp. 29067–29077, 2018, doi: 10.1109/ACCESS.2018.2826015.

[26] P. K. Ray and A. Mohanty, "A robust firefly–swarm hybrid optimization for frequency control in wind/PV/FC based microgrid," *Appl. Soft Comput.*, vol. 85, Dec. 2019, Art. no. 105823, doi: 10.1016/j.asoc.2019.105823.

[27] A. H. Alattar, S. I. Selem, H. M. B. Metwally, A. Ibrahim, R. Aboelsaud, M. A. Tolba, and A. M. El-Rifaie, "Performance enhancement of micro grid system with SMES storage system based on mine blast optimization algorithm," *Energies*, vol. 12, no. 16, p. 3110, Aug. 2019, doi: 10.3390/en12163110.

[28] S. Ranjan, D. C. Das, A. Latif, and N. Sinha, "LFC for autonomous hybrid micro grid system of 3 unequal renewable areas using mine blast algorithm," *Int. J. Renew. Energy Res.*, vol. 8, no. 3, pp. 1297–1308, 2018, doi: 10.20508/ijrer.v8i3.7732.g7429.

[29] P. Sanki, S. Mazumder, M. Basu, P. Sarathi, and P. Debapriya, "Moth flame optimization based fuzzy-PID controller for power–frequency balance of an islanded microgrid," *J. Inst. Eng. B*, vol. 102, no. 5, pp. 997–1006, 2021, doi: 10.1007/s40031-021-00607-4.

[30] D. Guha, P. K. Roy, and S. Banerjee, "Load frequency control of interconnected power system using grey wolf optimization," *Swarm Evol. Comput.*, vol. 27, pp. 97–115, Apr. 2016, doi: 10.1016/j.swevo.2015.10.004.

[31] D. Guha, P. K. Roy, and S. Banerjee, "Whale optimization algorithm applied to load frequency control of a mixed power system considering nonlinearities and PLL dynamics," *Energy Syst.*, vol. 11, no. 3, pp. 699–728, Aug. 2020, doi: 10.1007/s12667-019-00326-2.

[32] P. C. Sahu, S. Mishra, R. C. Prusty, and S. Panda, "Improved-salp swarm optimized type-II fuzzy controller in load frequency control of multi area islanded AC microgrid," *Sustain. Energy, Grids Netw.*, vol. 16, pp. 380–392, Dec. 2018, doi: 10.1016/j.segan.2018.10.003.

[33] M. Babaei, A. Abazari, and S. M. Muyeen, "Coordination between demand response programming and learning-based FOPID controller for alleviation of frequency excursion of hybrid microgrid," *Energies*, vol. 13, no. 2, pp. 442–465, 2020, doi: 10.3390/en13020442.

[34] H. Bevrani, F. Habibi, P. Babahajyani, M. Watanabe, and Y. Mitani, "Intelligent frequency control in an AC microgrid: Online PSO-based fuzzy tuning approach," *IEEE Trans. Smart Grid*, vol. 3, no. 4, pp. 1935–1944, Dec. 2012, doi: 10.1109/TSG.2012.2196806.

[35] D.-J. Lee and L. Wang, "Small-signal stability analysis of an autonomous hybrid renewable energy power generation/energy storage system. Part I: Time-domain simulations," *IEEE Trans. Energy Convers.*, vol. 23, no. 1, pp. 311–320, Mar. 2008, doi: 10.1109/TEC.2007.914309.

[36] L. Ortiz, J. W. González, L. B. Gutierrez, and O. Llanes-Santiago, "A review on control and fault-tolerant control systems of AC/DC microgrids," *Heliyon*, vol. 6, no. 8, pp. 511–528, 2020, doi: 10.1016/j.heliyon.2020.e04799.

[37] H. Bevrani, G. Ledwich, and J. J. Ford, "On the use of df/dt in power system emergency control," in *Proc. IEEE/PES Power Syst. Conf. Expo.*, Seattle, WA, USA, Mar. 2009, pp. 1–6, doi: 10.1109/PSCE.2009.4840173.

[38] A. Abazari, H. Monsef, and B. Wu, "Coordination strategies of distributed energy resources including FESS, DEG, FC and WTG in load frequency control (LFC) scheme of hybrid isolated micro-grid," *Int. J. Electr. Power Energy Syst.*, vol. 109, pp. 535–547, Jul. 2019, doi: 10.1016/j.ijepes.2019.02.029.

[39] S. Duryea, S. Islam, and W. Lawrance, "A battery management system for stand-alone photovoltaic energy systems," *IEEE Ind. Appl. Mag.*, vol. 7, no. 3, pp. 67–72, May/Jun. 2001, doi: 10.1109/2943.922452.

[40] U. Akram, R. Shah, and N. Mithulananthan, "Hybrid energy stoarage system for frequency regulation in microgrids with source and load uncertainties," *IET Gener., Transmiss. Distrib.*, vol. 13, no. 22, pp. 5048–5057, Nov. 2019, doi: 10.1049/iet-gtd.2018.7064.

[41] H. A. Yousef, *Power System Load Frequency Control*, 1st ed. Boca Raton, FL, USA: CRC Press, 2017, doi: 10.1201/9781315166292.

[42] A. K. Barik and D. C. Das, "Expeditious frequency control of solar photovoltaic/biogas/biodiesel generator based isolated renewable microgrid using grasshopper optimisation algorithm," *IET Renew. Power Gener.*, vol. 12, no. 14, pp. 1659–1667, Oct. 2018, doi: 10.1049/iet-rpg.2018.5196.

[43] V. Veerasamy, N. I. A. Wahab, R. Ramachandran, M. L. Othman, H. Hizam, A. X. R. Irudayaraj, J. M. Guerrero, and J. S. Kumar, "A Hankel matrix based reduced order model for stability analysis of hybrid power system using PSO-GSA optimized cascade PI-PD controller for automatic load frequency control," *IEEE Access*, vol. 8, pp. 71422–71446, 2020, doi: 10.1109/ACCESS.2020.2987387.

[44] M. E. Lotfy, T. Senjyu, M. A. Farahat, A. F. Abdel-Gawad, and A. Yona, "Enhancement of a small power system performance using multi-objective optimization," *IEEE Access*, vol. 5, pp. 6212–6224, 2017, doi: 10.1109/ACCESS.2017.2692879.

[45] A. Abazari, M. G. Dozein, and H. Monsef, "A new load frequency control strategy for an AC micro-grid: PSO-based fuzzy logic controlling approach," in *Proc. Smart Grid Conf. (SGC)*, Sanandaj, Iran, Nov. 2018, pp. 1–7, doi: 10.1109/SGC.2018.8777791.

[46] A. M. Hussien, R. A. Turky, H. M. Hasanien, and A. Al-Durra, "LMSRE-based adaptive PI controller for enhancing the performance of an autonomous operation of microgrids," *IEEE Access*, vol. 9, pp. 90577–90586, 2021, doi: 10.1109/ACCESS.2021.3091496.

[47] M. Pluhacek, R. Senkerik, I. Zelinka, and D. Davendra, "Designing PID controllers by means of PSO algorithm enhanced by various chaotic maps," in *Proc. 8th EUROSIM Congr. Modelling Simulation (EUROSIM)*, Cardiff, U.K., Sep. 2013, pp. 19–23, doi: 10.1109/EUROSIM.2013.14.

[48] P. Domański, *Control Performance Assessment: Theoretical Analyses and Industrial Practice*. Cham, Switzerland: Springer, 2020, doi: 10.1007/978-3-030-23593-2.

[49] Y. Arya, "A new optimized fuzzy FOPI-FOPD controller for automatic generation control of electric power systems," *J. Franklin Inst.*, vol. 356, no. 11, pp. 5611–5629, Jul. 2019, doi: 10.1016/j.jfranklin.2019.02.034.

[50] W. Tasnin and L. C. Saikia, "Maiden application of an sine–cosine algorithm optimised FO cascade controller in automatic generation control of multi-area thermal system incorporating dish-Stirling solar and geothermal power plants," *IET Renew. Power Gener.*, vol. 12, no. 5, pp. 585–597, Apr. 2018, doi: 10.1049/iet-rpg.2017.0063.

[51] A. Behera, T. K. Panigrahi, P. K. Ray, and A. K. Sahoo, "A novel cascaded PID controller for automatic generation control analysis with renewable sources," *IEEE/CAA J. Autom. Sinica*, vol. 6, no. 6, pp. 1438–1451, Nov. 2019, doi: 10.1109/JAS.2019.1911666.

[52] R. T. Marler and J. S. Arora, "Survey of multi-objective optimization methods for engineering," *Struct. Multidisciplinary Optim.*, vol. 26, no. 6, pp. 369–395, Mar. 2004, doi: 10.1007/s00158-003-0368-6.

[53] O. Grodzevich and O. Romanko, "Normalization and other topics in multi-objective optimization," in *Proc. Fields-MITACS Ind. Problems Workshop (FMIPW)*, vol. 2, Toronto, ON, Canada, Aug. 2006, pp. 89–101.

[54] S. Boyd and L. Vandenberghe, *Convex Optimization*. New York, NY, USA: Cambridge Univ. Press, 2004.

[55] D. Izci, S. Ekinci, M. Kayri, and E. Eker, "A novel improved arithmetic optimization algorithm for optimal design of PID controlled and Bode's ideal transfer function based automobile cruise control system," *Evolving Syst.*, vol. 13, no. 3, pp. 453–468, Jun. 2022, doi: 10.1007/s12530-021-09402-4.

[56] D. Izci, S. Ekinci, E. Eker, and M. Kayri, "Augmented hunger games search algorithm using logarithmic spiral opposition-based learning for function optimization and controller design," *J. King Saud Univ., Eng. Sci.*, pp. 1–9, Mar. 2022, doi: 10.1016/j.jksues.2022.03.001.

[57] L. Wang, Q. Cao, Z. Zhang, S. Mirjalili, and W. Zhao, "Artificial rabbits optimization: A new bio-inspired meta-heuristic algorithm for solving engineering optimization problems," *Eng. Appl. Artif. Intell.*, vol. 114, Sep. 2022, Art. no. 105082, doi: 10.1016/j.engappai.2022.105082.

[58] *Rabbit Free Photo by Amethyst*. Accessed: Oct. 1, 2022. [Online]. Available: https://www.freeimages.com/photo/the-rabbit-1363382

A. ELSAWY KHALIL was born in Egypt, in October 1990. He received the B.Sc. and M.Sc. degrees in electrical power and machines engineering from Cairo University, Egypt, in 2012 and 2017, respectively, where he is currently pursuing the Ph.D. degree in electrical engineering. Since 2013, he has been a Demonstrator with Cairo University. In 2017, he became a Research Assistant with Cairo University. His research interests include optimization, utilization and generation of electric power, distributed generation, and renewable energy sources.

TAREK A. BOGHDADY was born in Egypt, in March 1982. He received the M.Sc. and Ph.D. degrees in electrical power and machines engineering from Cairo University, Egypt, in 2011 and 2016, respectively. From 2005 to 2016, he was a Teaching Assistant at Cairo University. In 2016, he became an Assistant Professor with Cairo University. In 2022, he became an Associate Professor. His research interests include optimization, neural networks, FACTS, HVDC, utilization and generation of electric power, distributed generation, and renewable energy sources.

M. H. ALHAM was born in Egypt, in May 1985. He received the B.Sc., M.Sc., and Ph.D. degrees in electric power engineering from Cairo University, in 2007, 2012, and 2016, respectively. Since August 2016, he has been an Assistant Professor with Cairo University. His research interests include power system economic operation, distributed generation, and renewable energy sources.

DOAA KHALIL IBRAHIM (Senior Member, IEEE) was born in Egypt, in December 1973. She received the M.Sc. and Ph.D. degrees in digital protection from Cairo University, Cairo, Egypt, in 2001 and 2005, respectively.

From 1996 to 2005, she was a Demonstrator and a Research Assistant at Cairo University. She became an Assistant Professor, an Associate Professor, and a Professor with Cairo University, in 2005, 2011, and December 2016, respectively. From 2005 to 2008, she contributed to a World Bank Project in Higher Education Development, Egypt. From January 2010 to June 2013, she contributed as an Expert in the Program of Continuous Improvement and Qualifying for Accreditation in Higher Education, Egypt. From July 2013 to November 2014, she contributed as an Expert for the technical office of the Project Management Unit (PMU), Ministry of Higher Education, Egypt. Her research interests include the digital protection of power systems, utilization and generation of electric power, distributed generation, and renewable energy sources.